

Manipulating and diagnosing electron beam with cross-plane coupling in transverse and longitudinal phase spaces

Seongyeol Kim

Pohang Accelerator Laboratory, Republic of Korea

May 20, 2026



Contents

❖ Motivation of beam manipulation and precise beam diagnostics

- For HEP applications and high-bright light sources
- Generative Phase Space Reconstruction technique (GPSR)

❖ 4D and 6D beam manipulation + GPSR-based diagnostics

- Flat and magnetized beam transformations @ AWA facility
- Detailed 6D phase space reconstruction @ PAL-XFEL facility

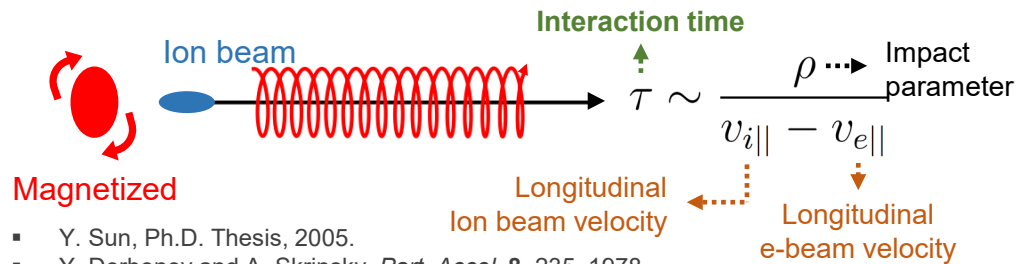
❖ Summary and future work



Motivation of beam manipulation

Use of magnetized beam:

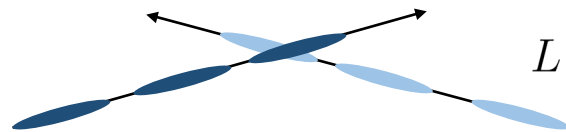
Reduction of hadron beam emittance: cooling



- Y. Sun, Ph.D. Thesis, 2005.
- Y. Derbenev and A. Skrinsky, *Part. Accel.* **8**, 235, 1978.

Use of flat beam:

Direct increases of luminosity



Small vertical beam size:
by flat beam with large magnetization

- K. Yokoya, P. Chen, Beam-beam phenomena in linear colliders, 2005.
- K. Buesser, Electron-Positron Linear Collider, 2009.

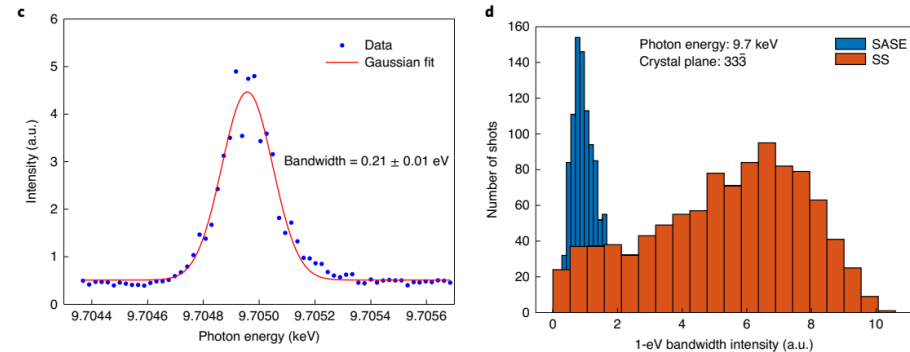
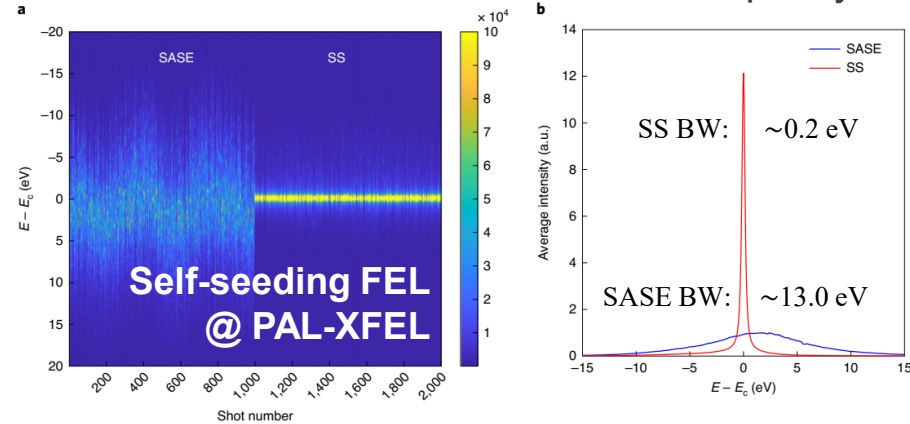
Luminosity

$$L \propto \frac{\eta_{RF} P_{RF}}{E_{cm}^{3/2}} \frac{\sqrt{\delta_{BS} \sigma_z}}{\sigma_y}$$

$$\epsilon_- \approx \frac{\epsilon_{th}^2}{2\mathcal{L}}$$

Use of refined electron beam*:

Enhancement of Free Electron Laser quality

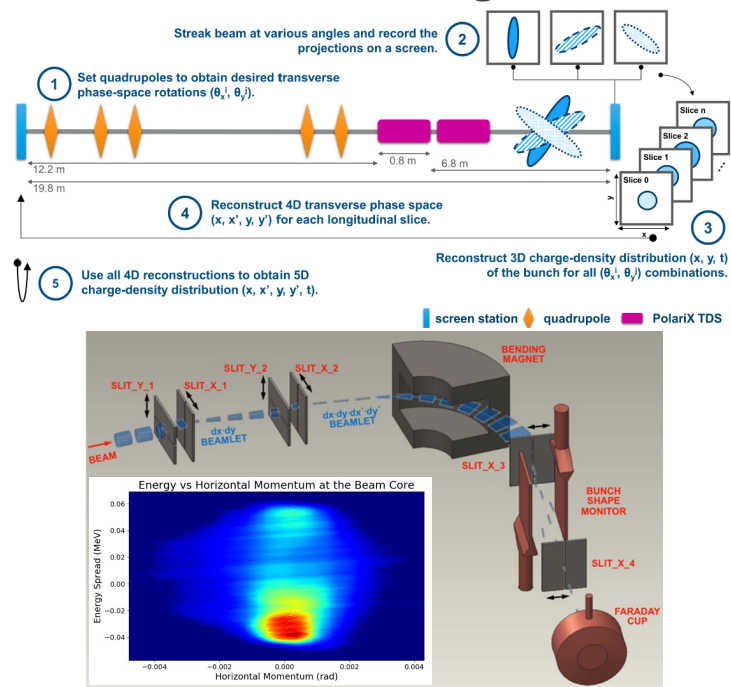


- H.-S. Kang et al., *Nat. Photonics* **11**, 2017.
- I. Nam et al., *Nat. Photonics* **15**, 2021.

For high-energy physics applications and high-brightness X-ray light:
Proper and accurate beam phase space manipulation is essential

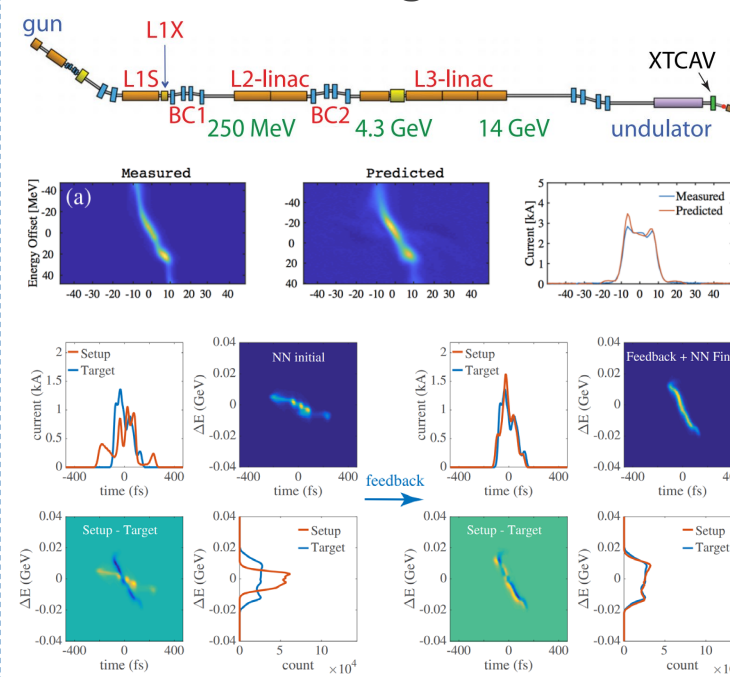
Beam diagnostics for characterizing manipulated beams

Conventional diagnostics



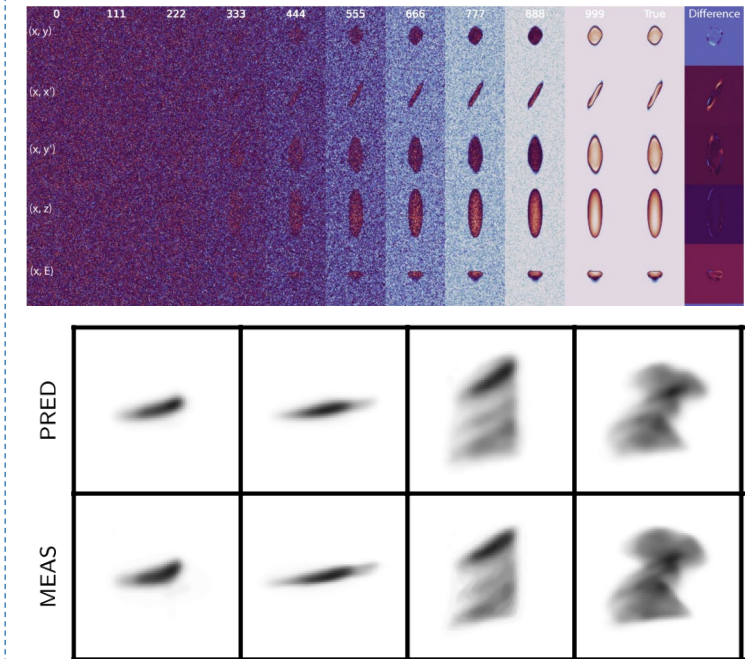
S. Jaster-Merz *et al.*, *PRAB* 27, 072801, 2024.
B. Cathey *et al.*, *PRL* 121, 064804, 2018.

Virtual diagnostics



C. Emma *et al.*, *PRAB* 21, 112802, 2018.
A. Scheinker *et al.*, *PRL* 121, 044801, 2018.

Generative learnings



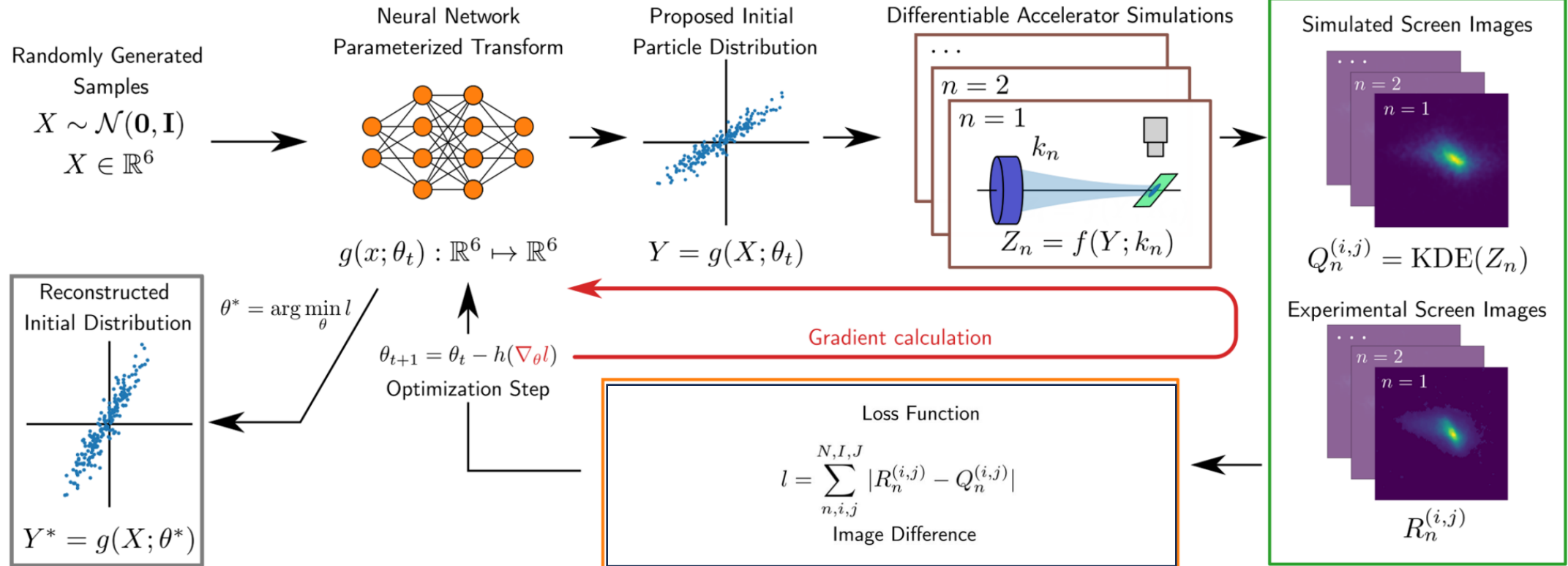
A. Scheinker, *Sci. Rep.* 14, 29303, 2024.
A. Hoover, *PRAB* 28, L084601, 2025.

Beam diagnostics from conventional approach to AI/ML technique-incorporated:
allows us to investigate phase space characterization in a robust way*

- R. Roussel *et al.*, *PRL* **130**, 145001, 2023.
- S. Kim *et al.*, *PRAB* **27**, 074601, 2024.
- R. Roussel *et al.*, *PRAB* **27**, 094601, 2024.
- J.P. Gonzalez-Aguilera *et al.*, *IPAC'24*, 2024.

Generative phase space reconstruction (GPSR)

Based on neural networks and differentiable simulations



Iteration process to update weights of neural networks:
To reconstruct beam phase space that successfully predicts experimental measurements

4D phase space manipulation and reconstruction

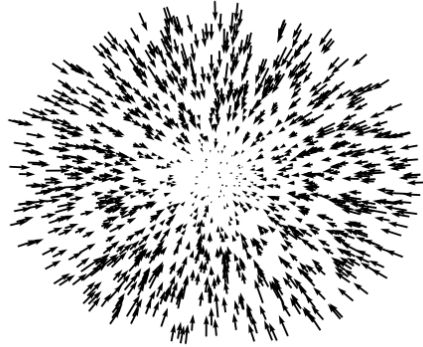
Based on:

- Seongyeol Kim *et al.*, *Phys. Rev. Accel. Beams* **27**, 074601, 2024.
- Seongyeol Kim *et al.*, *Nucl. Inst. Meth. Phys. Res. A* **1072**, 170206, 2025.



What are flat and magnetized beams?

Round beam



Typical beam we use (does not rotate)

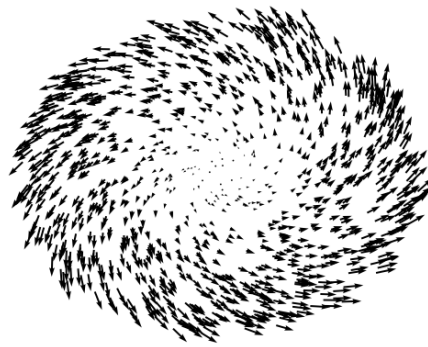
Solenoid field at the cathode
 $\mathbf{P} = \mathbf{p} + e\mathbf{A} = \mathbf{p} + \frac{B_c}{2}(-y\hat{x} + x\hat{y})$



$$\mathbf{L} = \mathbf{r} \times \mathbf{P}$$

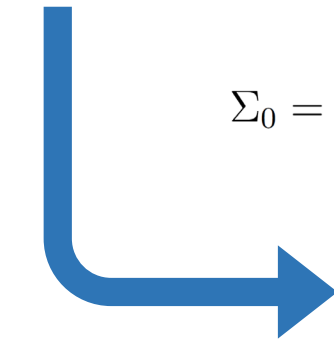
Canonical Angular momentum

Round, magnetized beam



Angular-momentum-dominated beam

$$\Sigma_0 = \begin{bmatrix} \epsilon_{eff}T_0 & \mathcal{L}J \\ -\mathcal{L}J & \epsilon_{eff}T_0 \end{bmatrix}$$



Magnetization

$$\mathcal{L} = \frac{\langle L \rangle}{2m_e c}$$

where $T_0 = \begin{bmatrix} \beta & -\alpha \\ \alpha & \gamma \end{bmatrix}$ $J = \begin{bmatrix} 0 & -1 \\ 1 & 0 \end{bmatrix}$



$$\Sigma_1 = M\Sigma_0M^\top$$

$$\Sigma_1 = \begin{bmatrix} \epsilon_+T_+ & 0 \\ 0 & \epsilon_-T_- \end{bmatrix}$$

Flat beam



Eigenemittance

$$\epsilon_+ \approx 2\mathcal{L} \quad \epsilon_- \approx \frac{\epsilon_{th}^2}{2\mathcal{L}}$$

ϵ_{th} Uncorrelated emittance

For magnetization = 50 μm , and $\epsilon_{th} = 5.0 \mu\text{m}$,

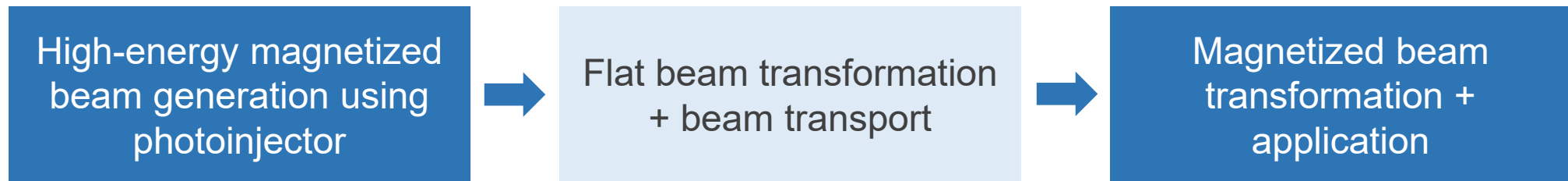
ϵ_+ (Emit_nx) (mm mrad)	ϵ_- (Emit_ny) (mm mrad)
100	0.25

Back-to-back beam transformations @ AWA facility

Back-to-back(B2B): Round-to-flat and flat-to-round(magnetized) beam transformations*

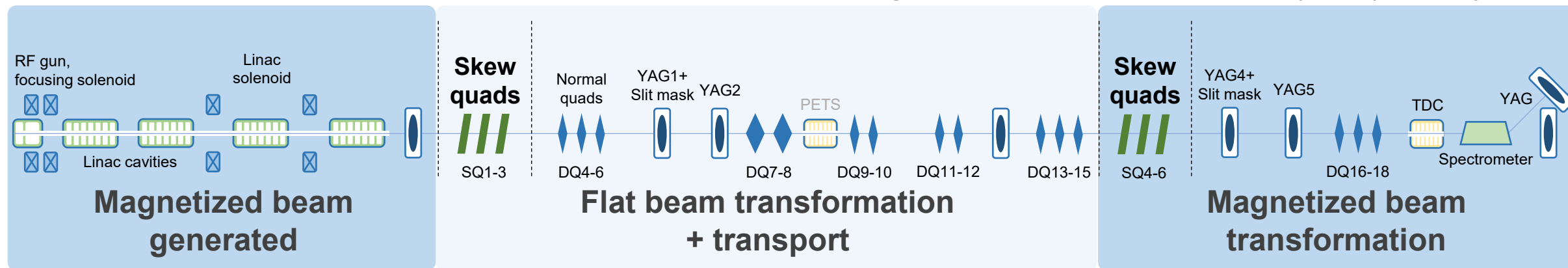
Motivation of beam transformations:

- Difficulty of high-energy* magnetized beam transport: make it easy by decoupling
- Then, transformation back to magnetized condition at the application section (e.g., cooling)

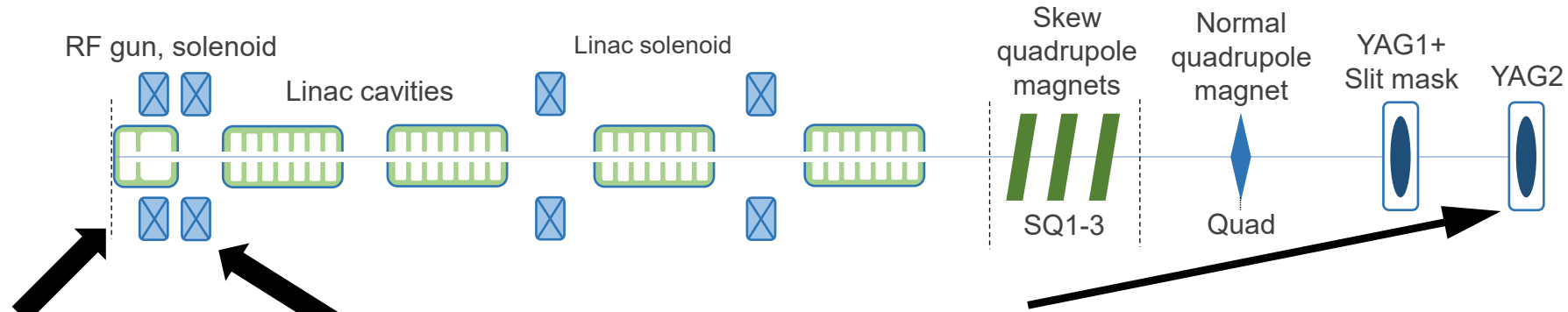


Goal of demonstration:

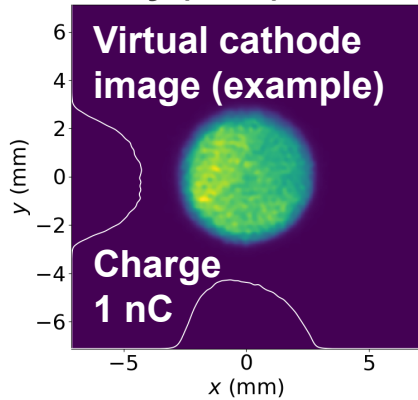
- Experimental demo of back-to-back transformations at Argonne Wakefield Accelerator (AWA) Facility



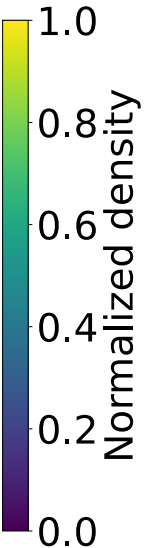
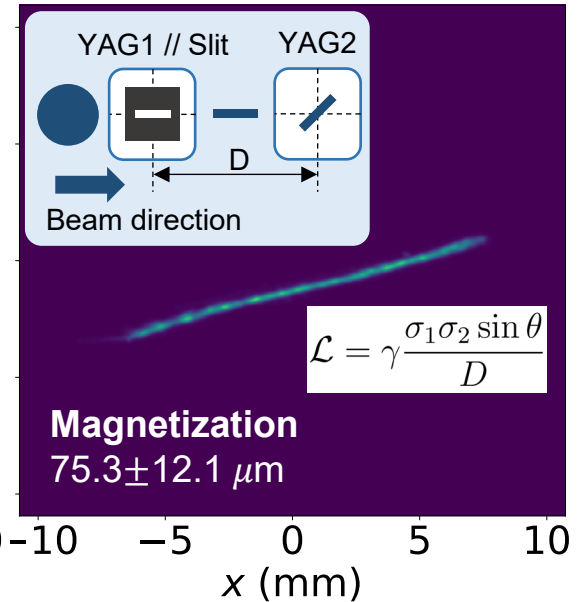
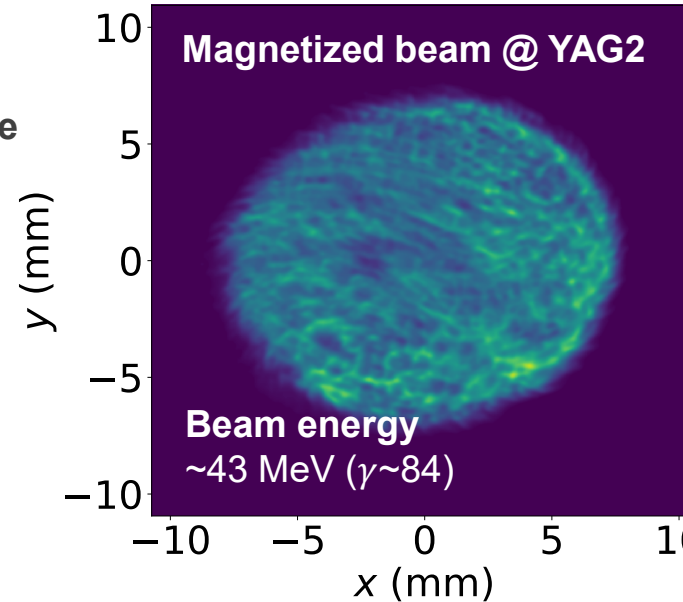
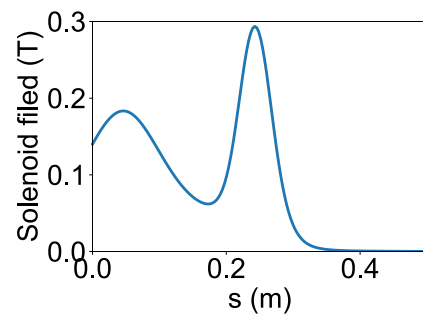
Experimental demonstration of beam transformations



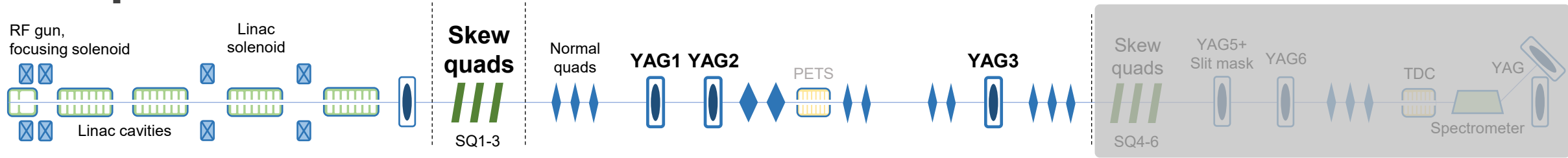
Use of multi-lens array (MLA)



No bucking solenoid: Non-zero B-field at cathode



Experimental demonstration of beam transformations



For magnetized beam: $\mathbf{Y} = C\mathbf{X}$
 $\mathbf{X} = (x, p_x), \mathbf{Y} = (y, p_y)$

Twiss Parameters

$$C = \frac{\mathcal{L}}{\epsilon_{eff}} \begin{bmatrix} \alpha & \beta \\ -\frac{1+\alpha^2}{\beta^2} & -\alpha \end{bmatrix}$$

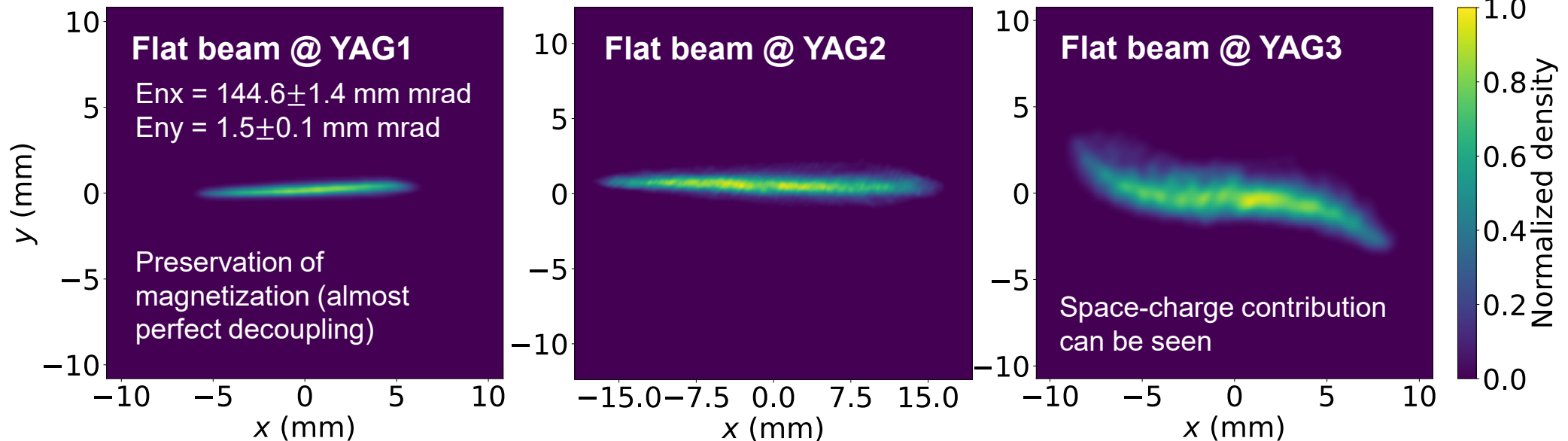
where $\epsilon_{eff} = \sqrt{\epsilon_{th}^2 + \mathcal{L}^2}$

RFBT matrix calculation

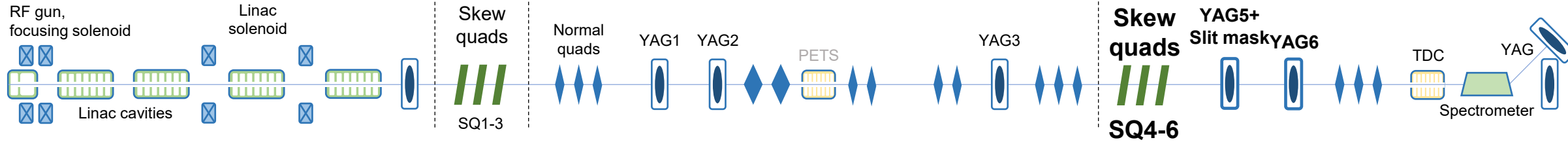
$$\begin{pmatrix} \mathbf{X} \\ \mathbf{Y} \end{pmatrix} = \frac{1}{2} \begin{pmatrix} [A + B + (A - B)C]\mathbf{X} \\ [A - B + (A + B)C]\mathbf{X} \end{pmatrix}$$

where skew triplet matrix, $M_{SQ} = \begin{pmatrix} A + B & A - B \\ A - B & A + B \end{pmatrix}$

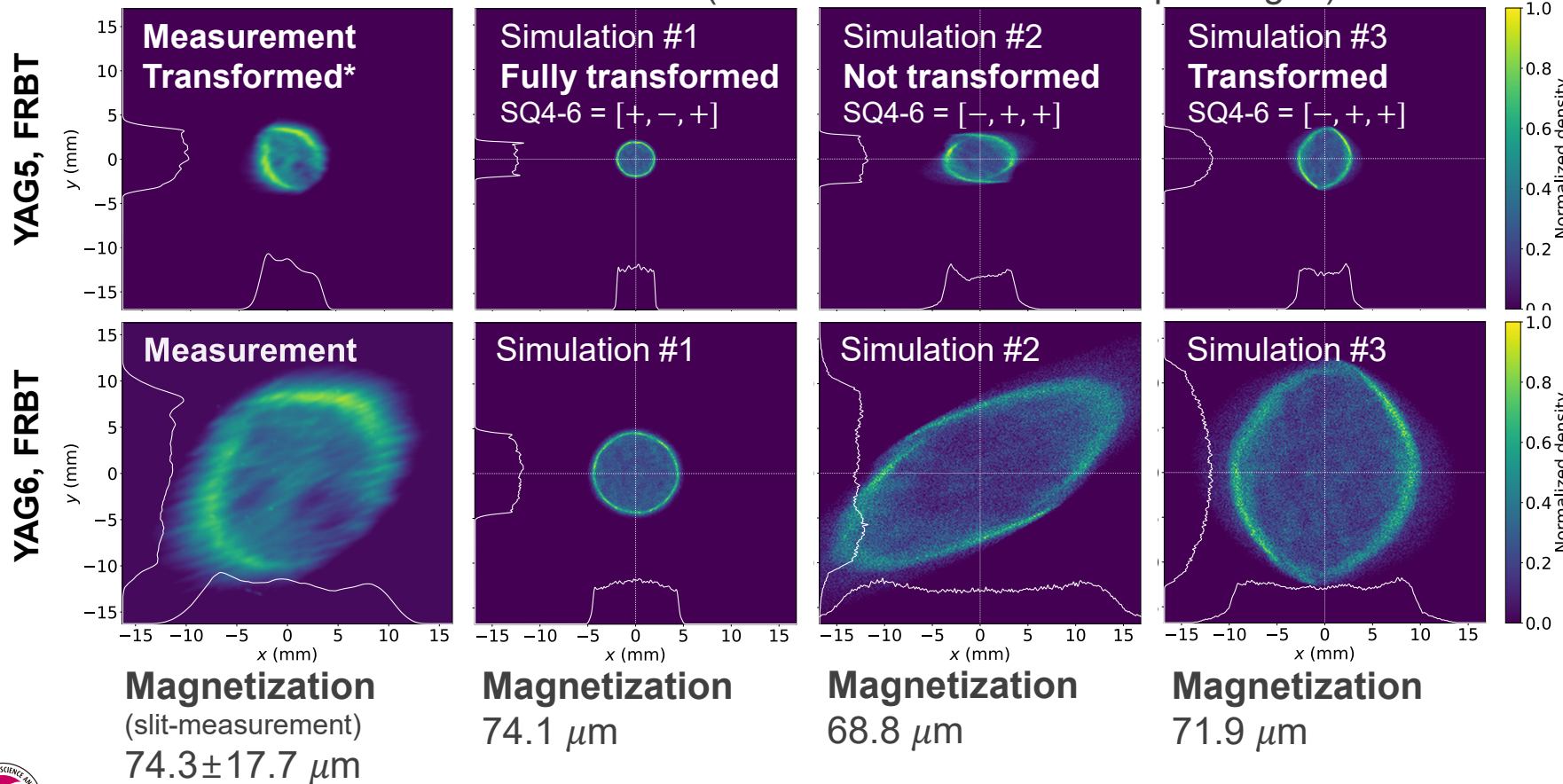
RFBT goal: find skew quad settings that vanishes \mathbf{Y}



Experimental demonstration of beam transformations



Flat to round beam transformation (simulations with different quad signs)



*For simulation #2,
 $|\gamma\langle xy' \rangle| \neq |\gamma\langle x'y \rangle|$
 Thus, not transformed

precise beam diagnostic method is required for accurate validation of transversely coupled beam!

↓

GPSR technique

Characterization of magnetized beam using GPSR

Different UV distribution and solenoid field were applied in this case

Magnetized beam matrix

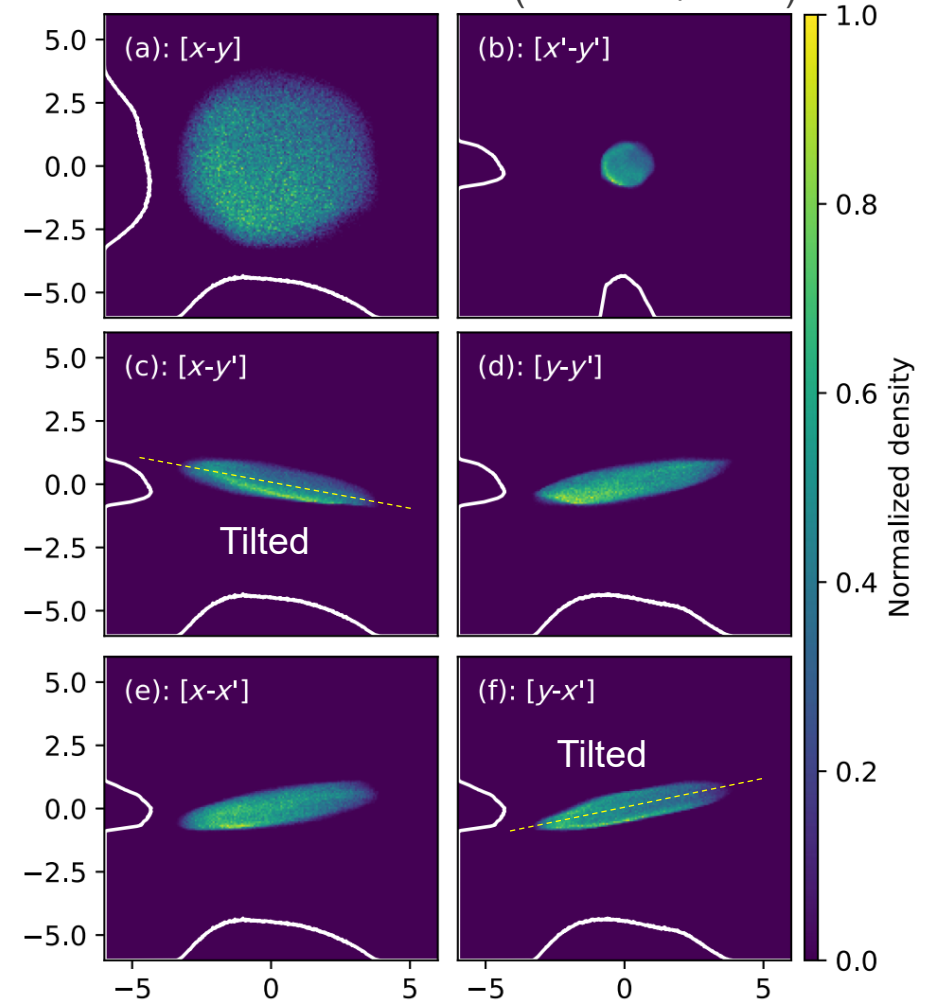
$$\begin{bmatrix} \epsilon_{eff}\beta_x & -\epsilon_{eff}\alpha_x & 0 & \mathcal{L} \\ -\epsilon_{eff}\alpha_x & \epsilon_{eff}\gamma_x & -\mathcal{L} & 0 \\ 0 & -\mathcal{L} & \epsilon_{eff}\beta_y & -\epsilon_{eff}\alpha_y \\ \mathcal{L} & 0 & -\epsilon_{eff}\alpha_y & \epsilon_{eff}\gamma_y \end{bmatrix} \rightarrow |\gamma (\langle xy' \rangle - \langle yx' \rangle)|/2$$

$$\epsilon_{eff} = \sqrt{\epsilon_{th}^2 + \mathcal{L}^2} \quad \beta, \alpha, \gamma: \text{Twiss parameters}$$

Magnetization, case	Value (um)
Reconstruction	44.0
Slit measurement	47.2 ± 0.9

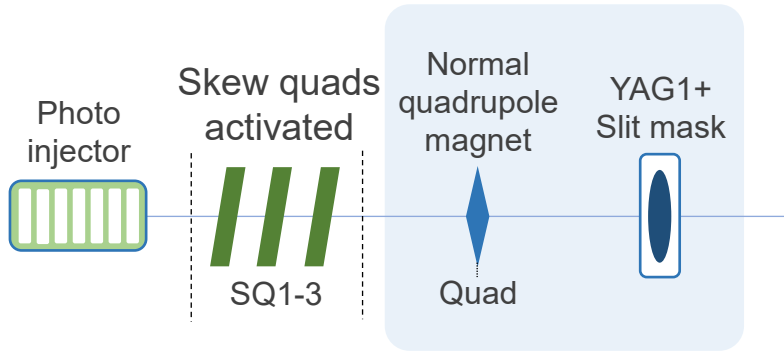
GPSR for magnetized beams:
Successful to obtain detailed phase space information including couplings

Reconstructed phase space
(unit: mm / mrad)



Characterization of flat beam using GPSR

Different UV distribution and solenoid field were applied (also compared to magnetized beam GPSR)

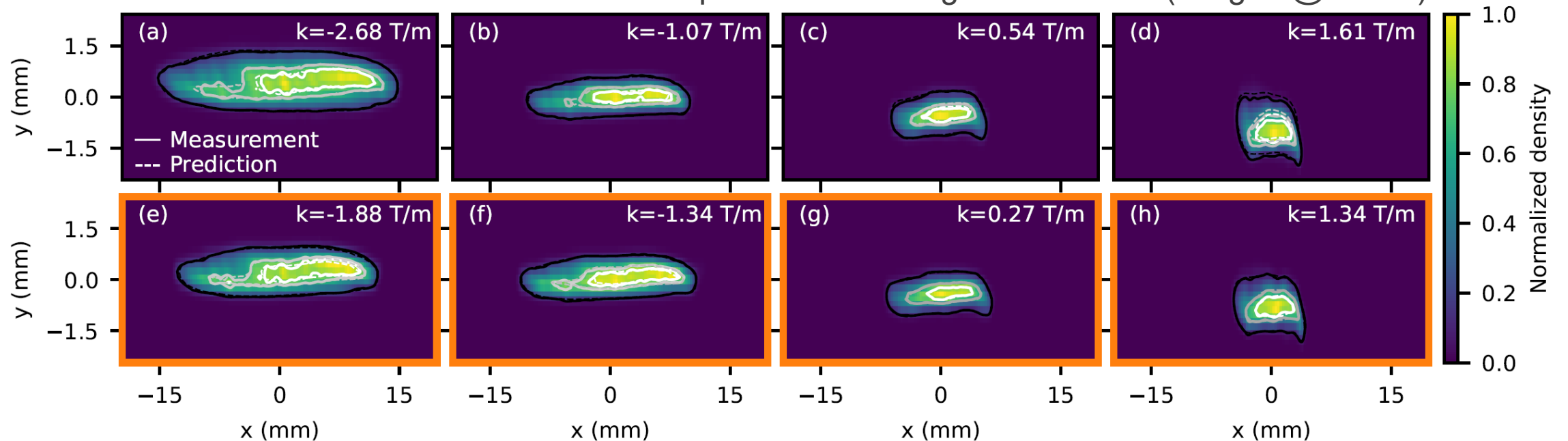


GPSR setup:

- 21 quadscan samples (half for train)
- 100k particles, 4000 epochs



Comparison of training / test dataset (images @ YAG1)



Characterization of flat beam using GPSR

Different UV distribution and solenoid field were applied (also compared to magnetized beam GPSR)

After beam transformation, beam covariance becomes:

$$\begin{bmatrix} \langle x^2 \rangle & \langle xx' \rangle & \langle xy \rangle & \langle xy' \rangle \\ \langle xx' \rangle & \langle x'^2 \rangle & \langle yx' \rangle & \langle x'y' \rangle \\ \langle xy \rangle & \langle xy' \rangle & \langle y^2 \rangle & \langle yy' \rangle \\ \langle yx' \rangle & \langle x'y' \rangle & \langle yy' \rangle & \langle y'^2 \rangle \end{bmatrix} = \begin{bmatrix} \epsilon_+ \beta_+ & -\epsilon_+ \alpha_+ & 0 & 0 \\ \epsilon_+ \alpha_+ & \epsilon_+ \gamma_+ & 0 & 0 \\ 0 & 0 & \epsilon_- \beta_- & -\epsilon_- \alpha_- \\ 0 & 0 & \epsilon_- \alpha_- & \epsilon_- \gamma_- \end{bmatrix}$$

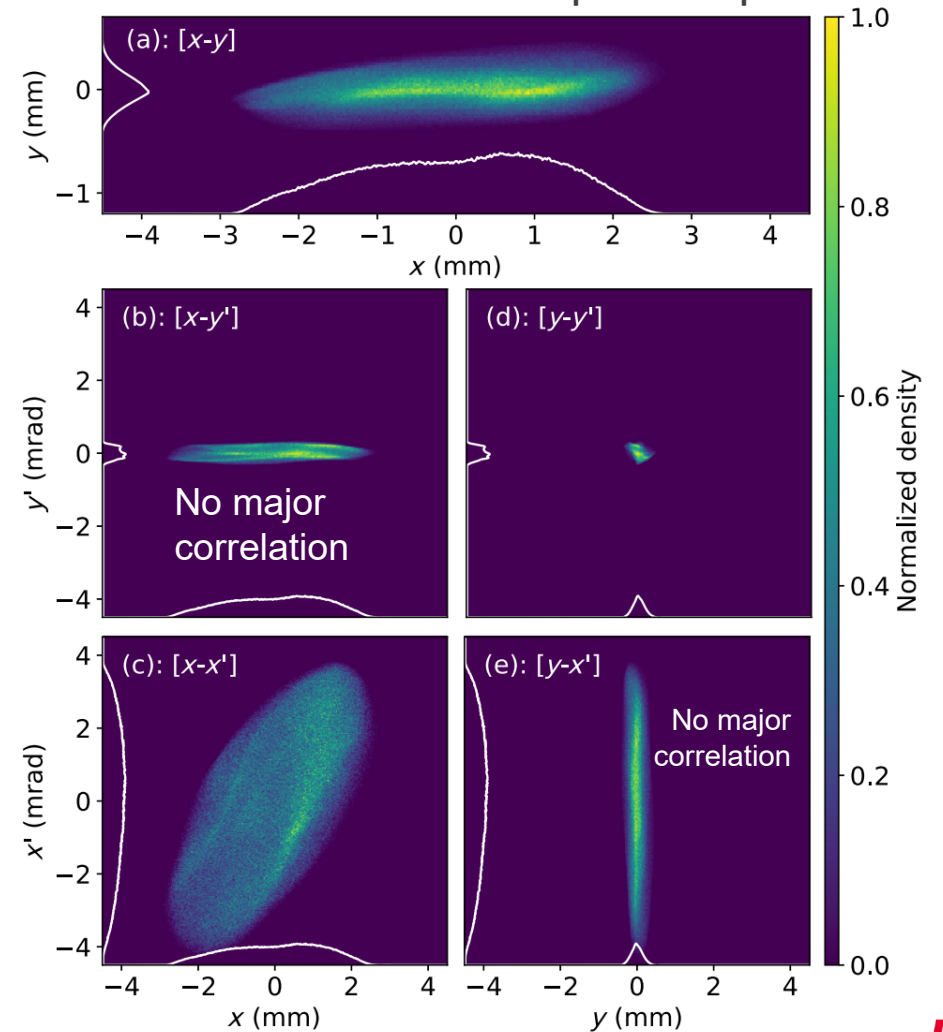
Where eigen-emittances:

$$\epsilon_+ \approx 2\mathcal{L} \quad \epsilon_- \approx \frac{\epsilon_{th}^2}{2\mathcal{L}} \quad \epsilon_{th} \text{ Uncorrelated emittance}$$

Case	Emit_nx (ϵ_+) (mm mrad)	Emit_ny (ϵ_-) (mm mrad)
Reconstruction	140.14	1.53
Measurement (Quadrupole scan)	144.64 ± 1.36	1.47 ± 0.10

Also, GPSR technique successfully reconstructed flat beams!

Reconstructed phase space



6D phase space manipulation and reconstruction

Based on:

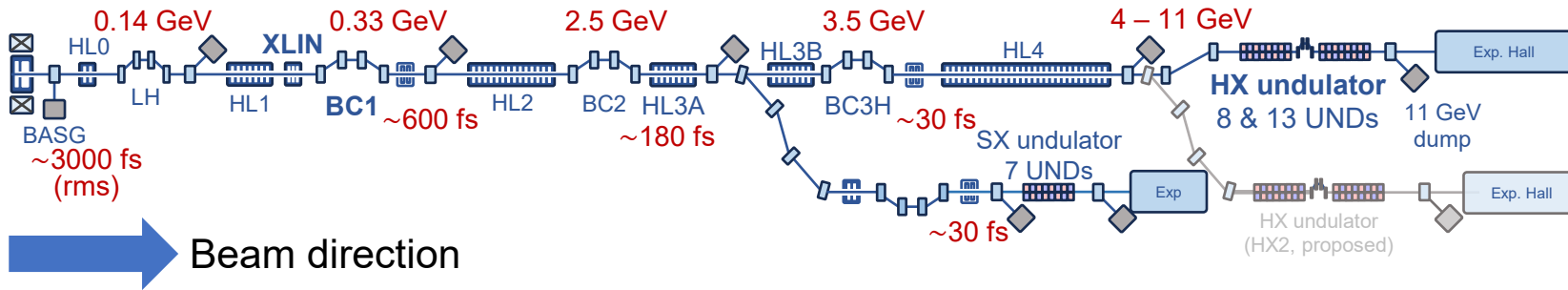
- Seongyeol Kim *et al.*, *Sci. Rep.* **15**, 43049, 2025.



Pohang Accelerator Laboratory, X-ray Free Electron Laser




PAL-XFEL Layout





Undulator Line	HX	SX
Photon energy (keV)	2.0~20.0	0.25~1.25
Beam energy (GeV)	4~11	3.0
Beam charge (pC)	190/250	160/250
Peak current (kA)	~3	~2.5
E_{ph} tuning	Energy/Gap	Gap
Repetition rate (Hz)	60	60
FEL intensity	> 1 mJ	> 250 μ J

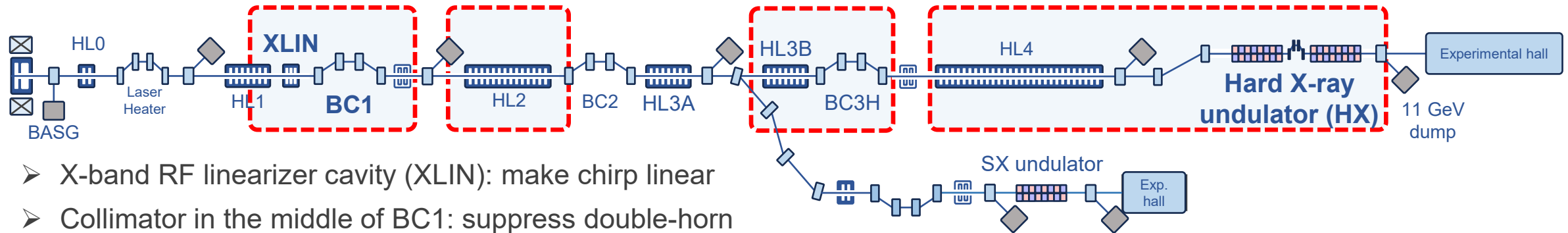
Beam manipulation @ PAL-XFEL HX

 S-band accelerating cavity (XLIN = X-band linearizer)

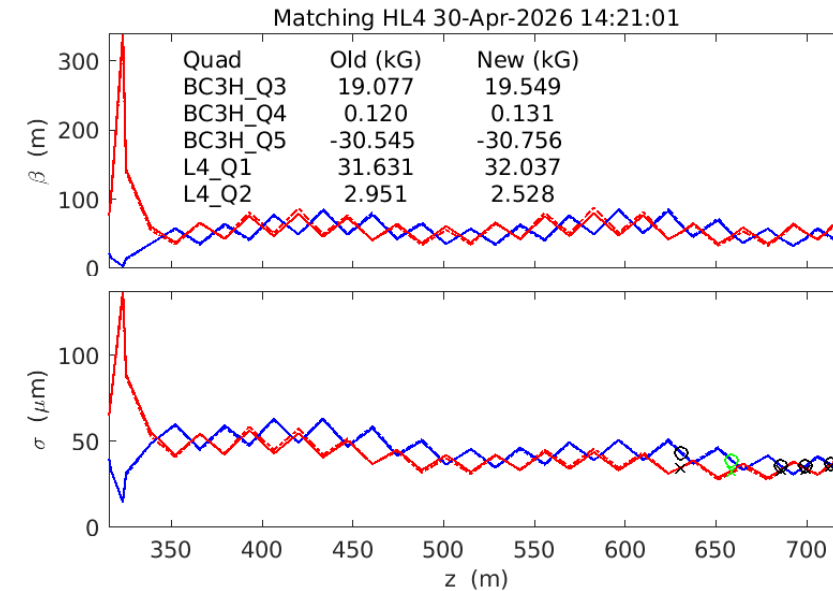
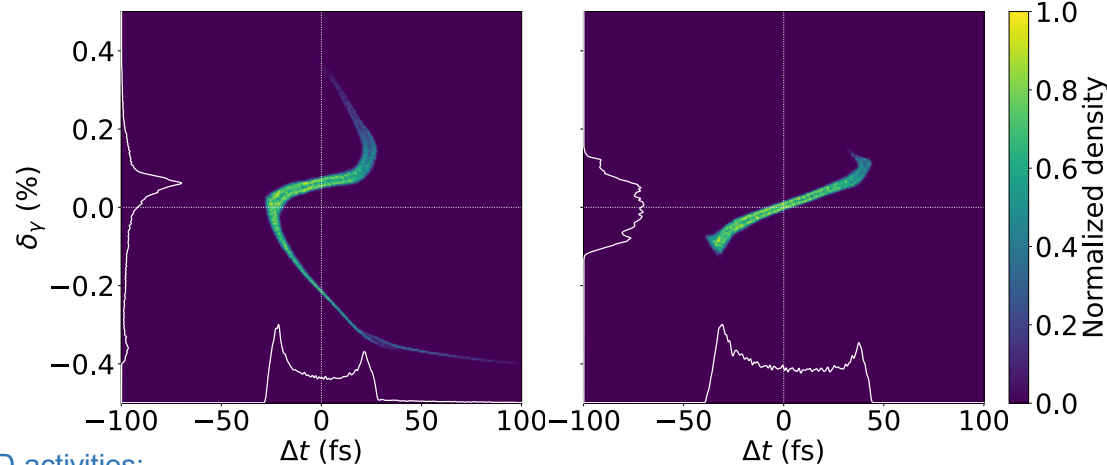
 Bunch compressor

 S-band transverse deflecting cavity (RF frequency = 2.856 GHz)

 BAS: dump spectrometer



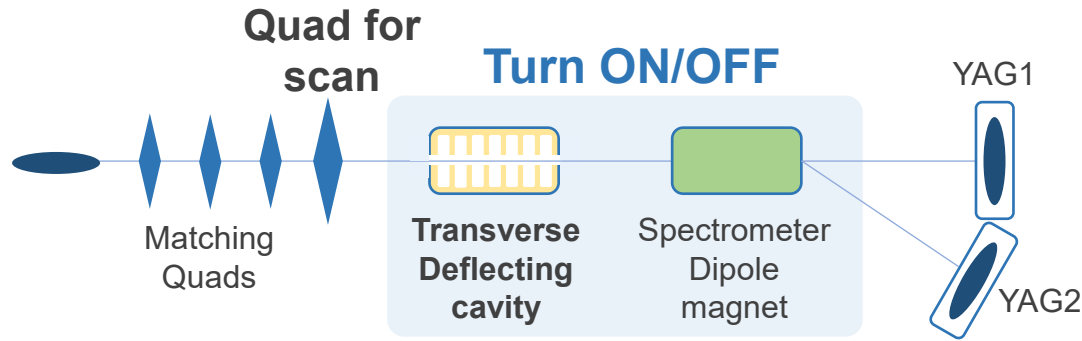
- X-band RF linearizer cavity (XLIN): make chirp linear
- Collimator in the middle of BC1: suppress double-horn
- BC3H: emittance optimization against CSR
- HL2, HL4, HX sections: FODO lattice matching



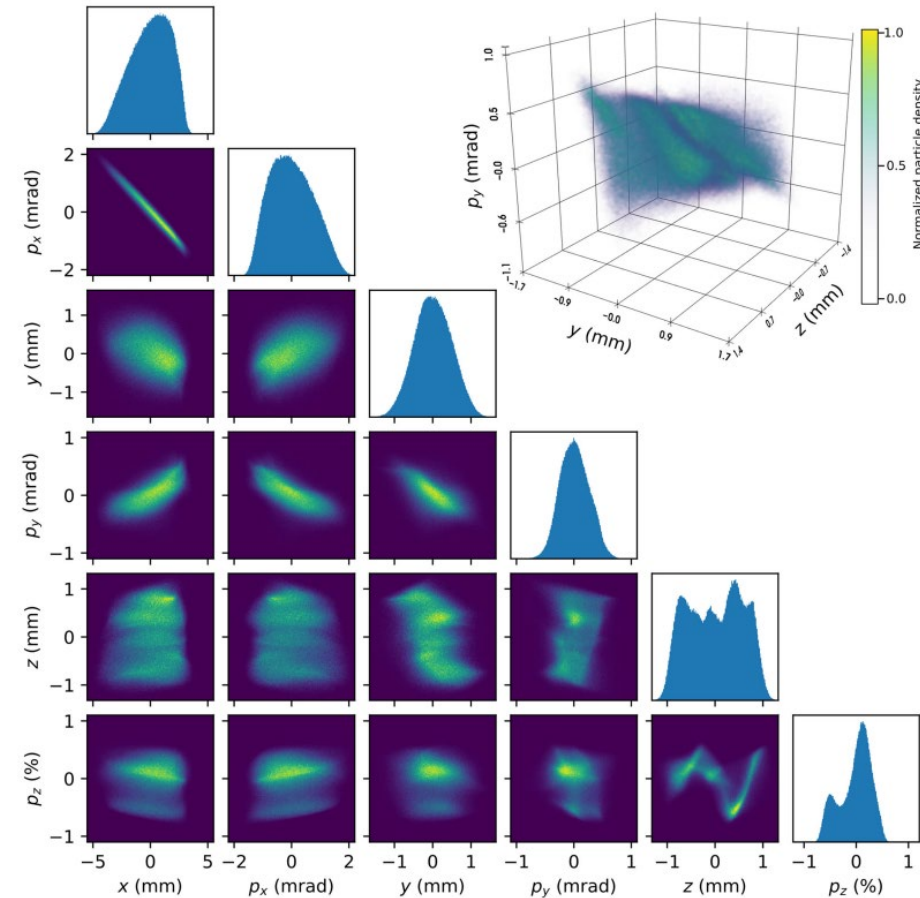
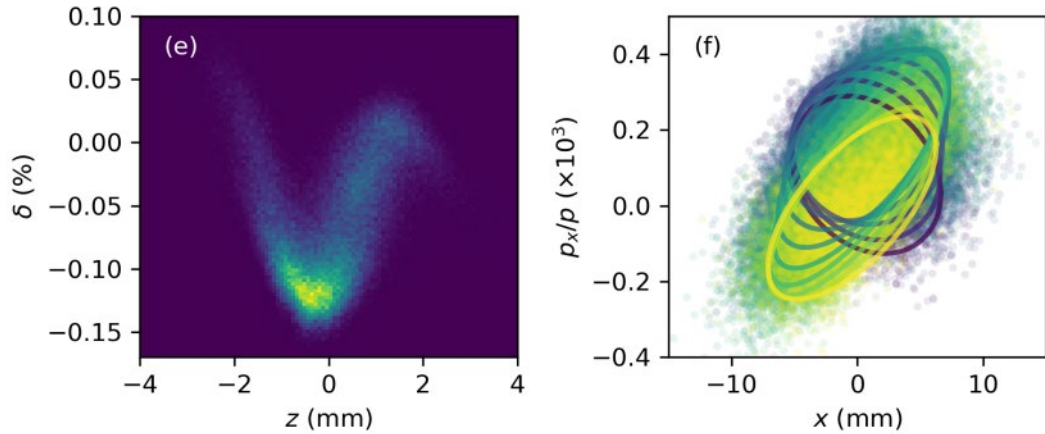
Other R&D activities:

- UV laser control: **Seong-Hoon Kwon et al., TUP7721 (Tuesday poster)**
- FEL mode development: **Chi Hyun Shim et al., TUP2662 (Tuesday poster)**
- Beam phase space diagnostics: **Myunghoon Cho et al., MOP6656 (Monday poster)**

6D GPSR using transverse deflecting cavity



CSR characterization



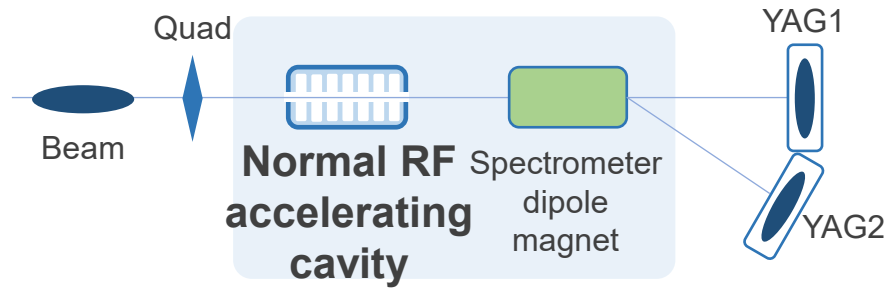
➔ **6-dimensional phase space reconstruction is also successfully performed and currently deployed @ LCLS-II, SLAC***

6D GPSR using RF accelerating cavity

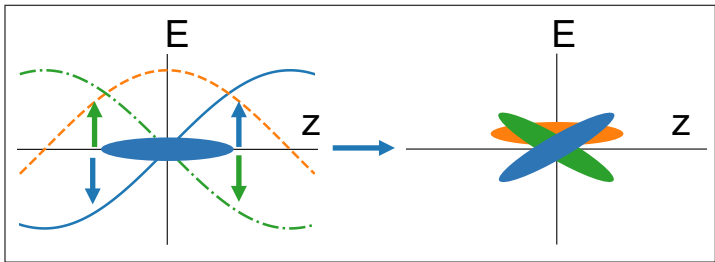
Inspired by conventional longitudinal emittance measurement*

*Longitudinal emittance:

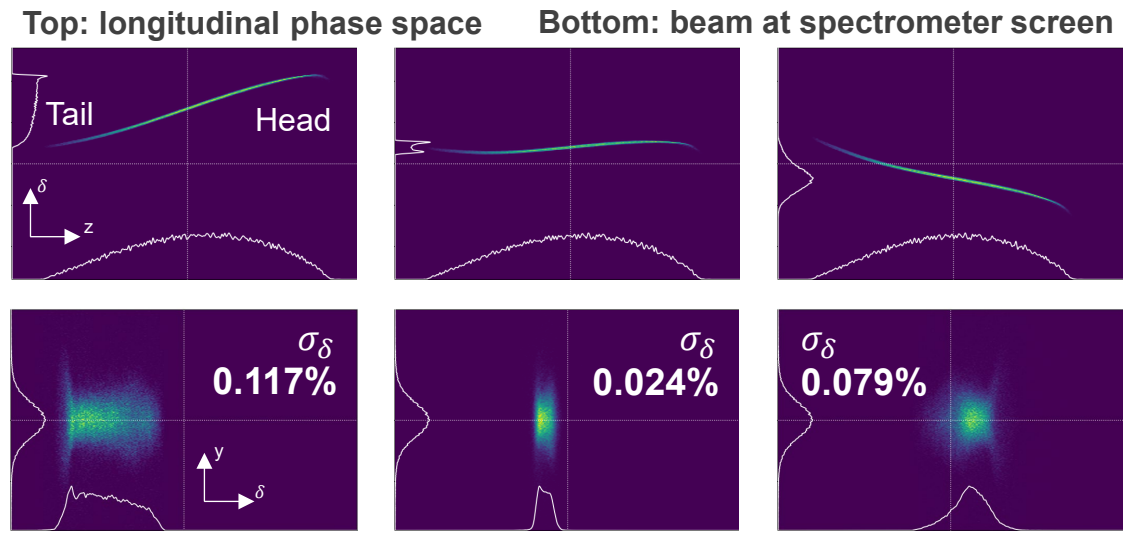
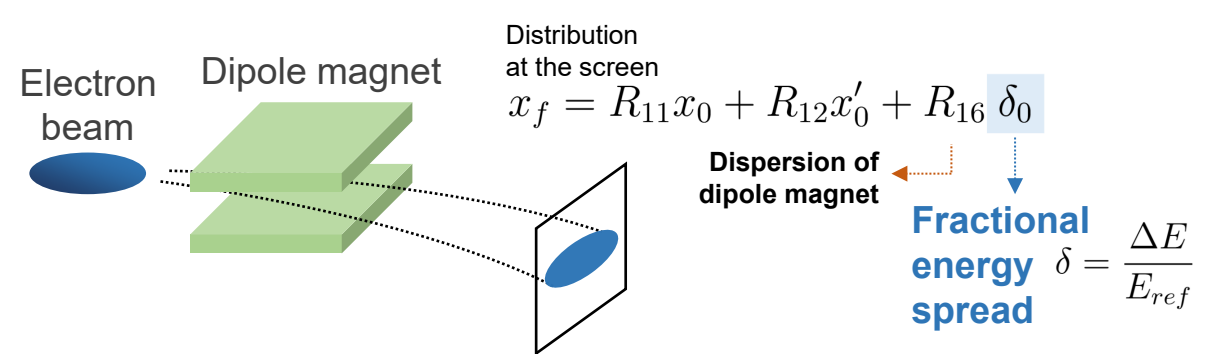
- D. Dowell et al., *In. Proc. PAC'03*, 2003.
 - D. Dowell et al., *Nucl. Inst. Meth. Phys. Res. A* **507**, 331, 2003.
- Longitudinal phase space tomography:
- H. Loos et al., *Nucl. Inst. Meth. Phys. Res. A* **528**, 189-193, 2004.



$$\Delta E(z) = eV \cos(k_{RF}z + \phi_{RF})$$



For a given longitudinal distribution:
➔ Energy changes induced by the cavity can be captured at the spectrometer screen



6D GPSR using RF accelerating cavity

Inspired by conventional longitudinal emittance measurement*

*Longitudinal emittance:

- D. Dowell et al., *In. Proc. PAC'03*, 2003.
 - D. Dowell et al., *Nucl. Inst. Meth. Phys. Res. A* **507**, 331, 2003.
- Longitudinal phase space tomography:
- H. Loos et al., *Nucl. Inst. Meth. Phys. Res. A* **528**, 189-193, 2004.

Transfer matrix for cavity and drift

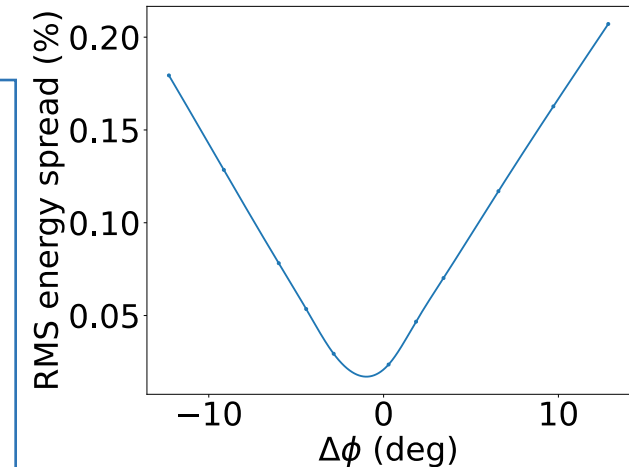
$$M = \begin{pmatrix} 1 & l \\ 0 & 1 \end{pmatrix} \begin{pmatrix} 1 & 0 \\ -V \sin(\phi_{RF}) & 1 \end{pmatrix} \quad \text{where} \quad \Sigma_i = \begin{pmatrix} \sigma_{11} & \sigma_{12} \\ \sigma_{21} & \sigma_{22} \end{pmatrix} = \begin{pmatrix} \langle z^2 \rangle & \langle z\delta \rangle \\ \langle z\delta \rangle & \langle \delta^2 \rangle \end{pmatrix}$$

$$\sigma_{22}^{YAG} = \sigma_{\delta}^2 = V^2 \sigma_{11} \phi^2 - 2V \sigma_{12} \phi + \sigma_{22}$$

RMS energy spread at the screen = $A\phi^2 + B\phi + C$ → Similar to normal quadscan: Estimation of second-order moments

$$\epsilon_z = \sqrt{\sigma_{11}\sigma_{12} - \sigma_{12}^2} \quad \rightarrow \quad \text{Emittance}$$

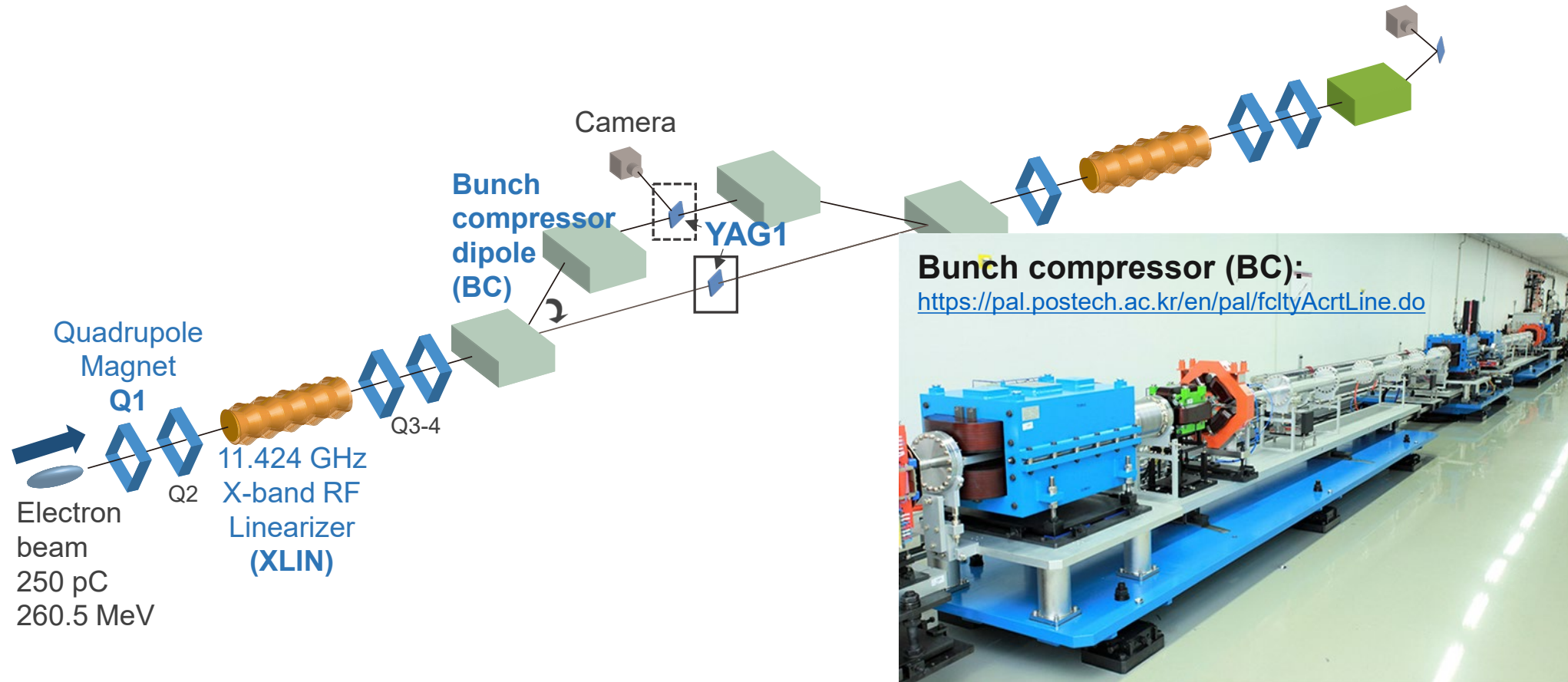
Example: Quadratic behavior of energy spread



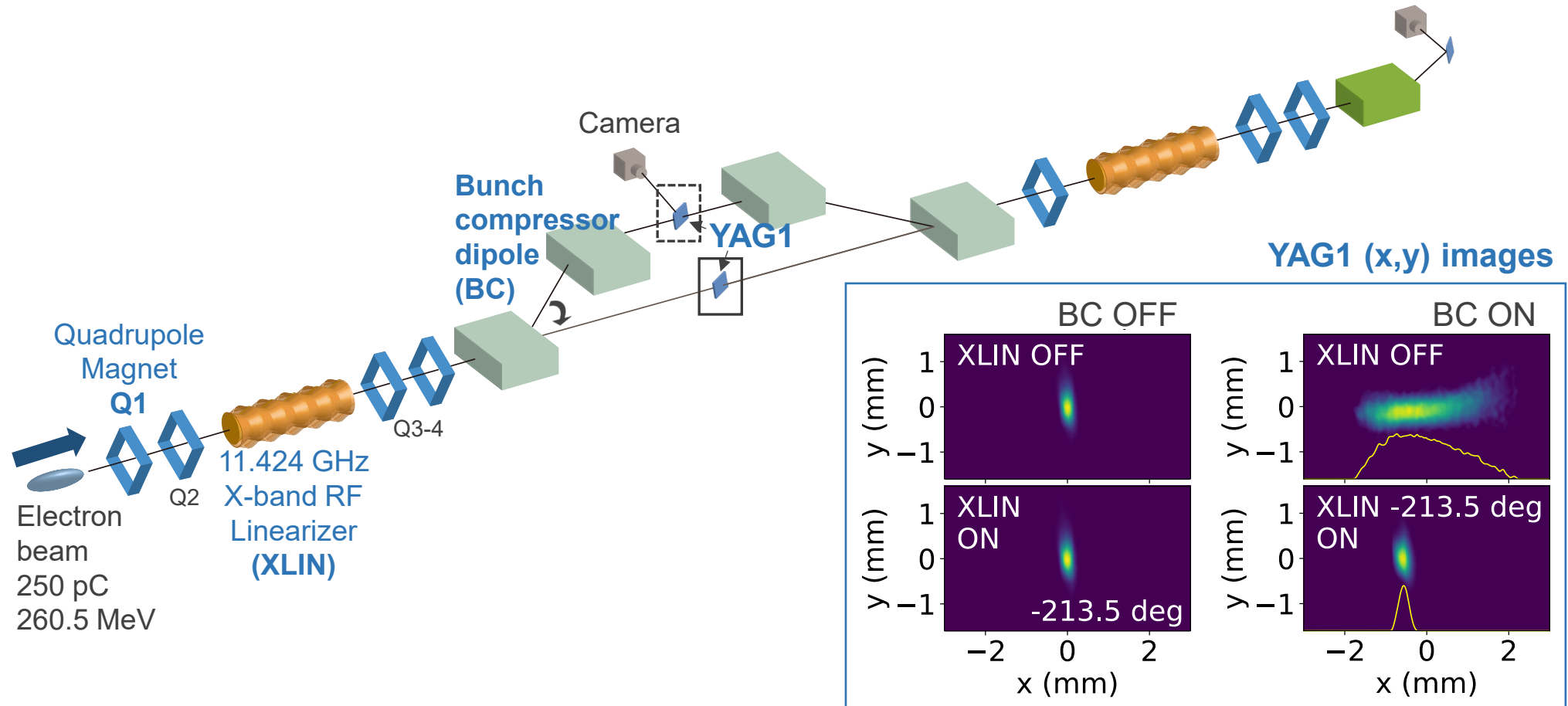
By combining quadrupole field and cavity phase scans, and GPSR:

We can obtain complete 6-dimensional coupled phase space of the beam

Experimental setup for the GPSR @ PAL-XFEL



Experimental setup for the GPSR @ PAL-XFEL

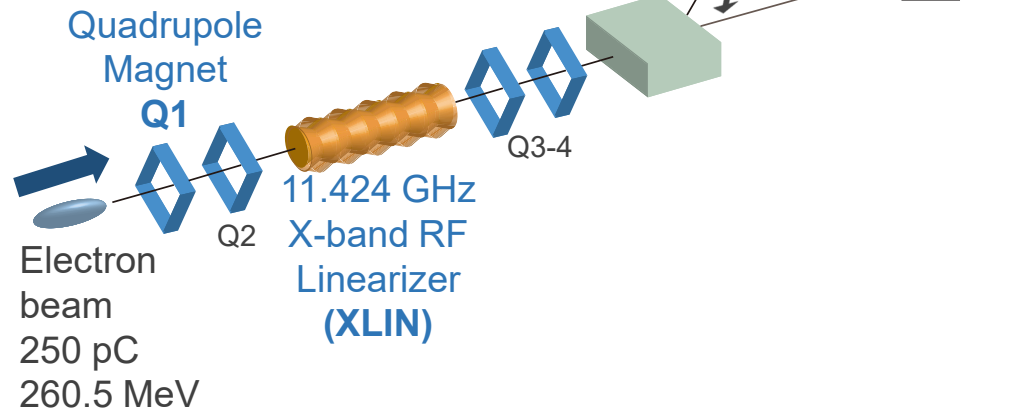


Experimental setup for the GPSR @ PAL-XFEL

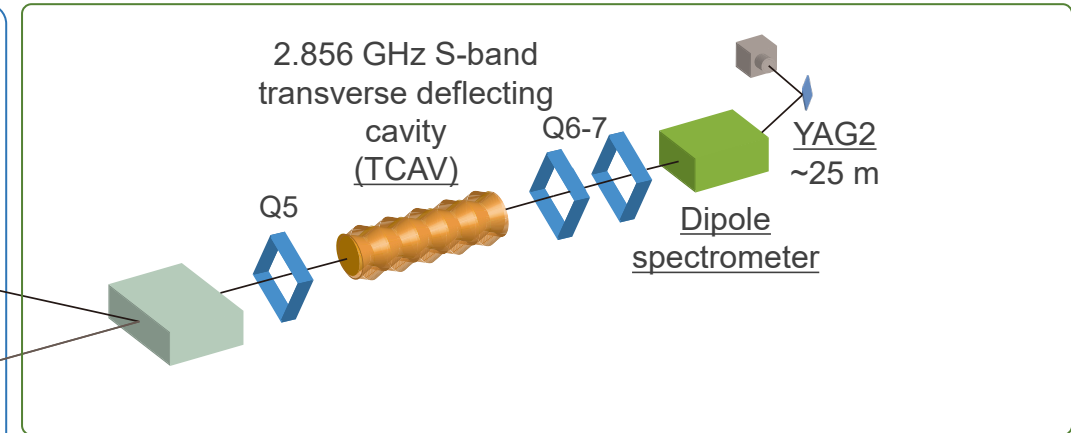


GPSR demo section

Parameters	# of samples
Quad strength	16
XLIN phase	5
BC condition	2
Total samples	160(80 for train)



GPSR validation section

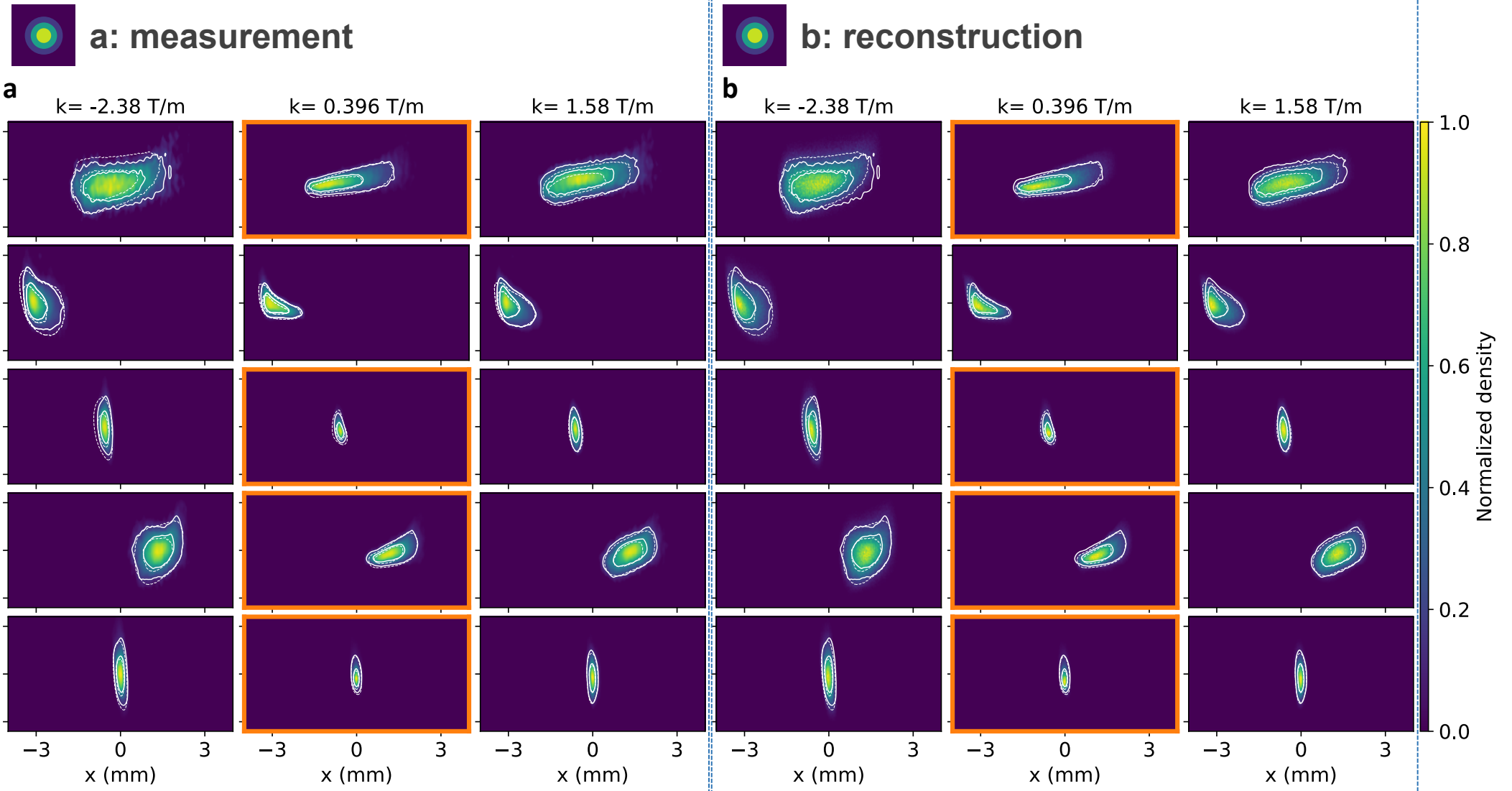


GPSR setup	Values
# of particles	100,000
# of iterations	1,000
Training time	~30 mins (Nvidia A100)

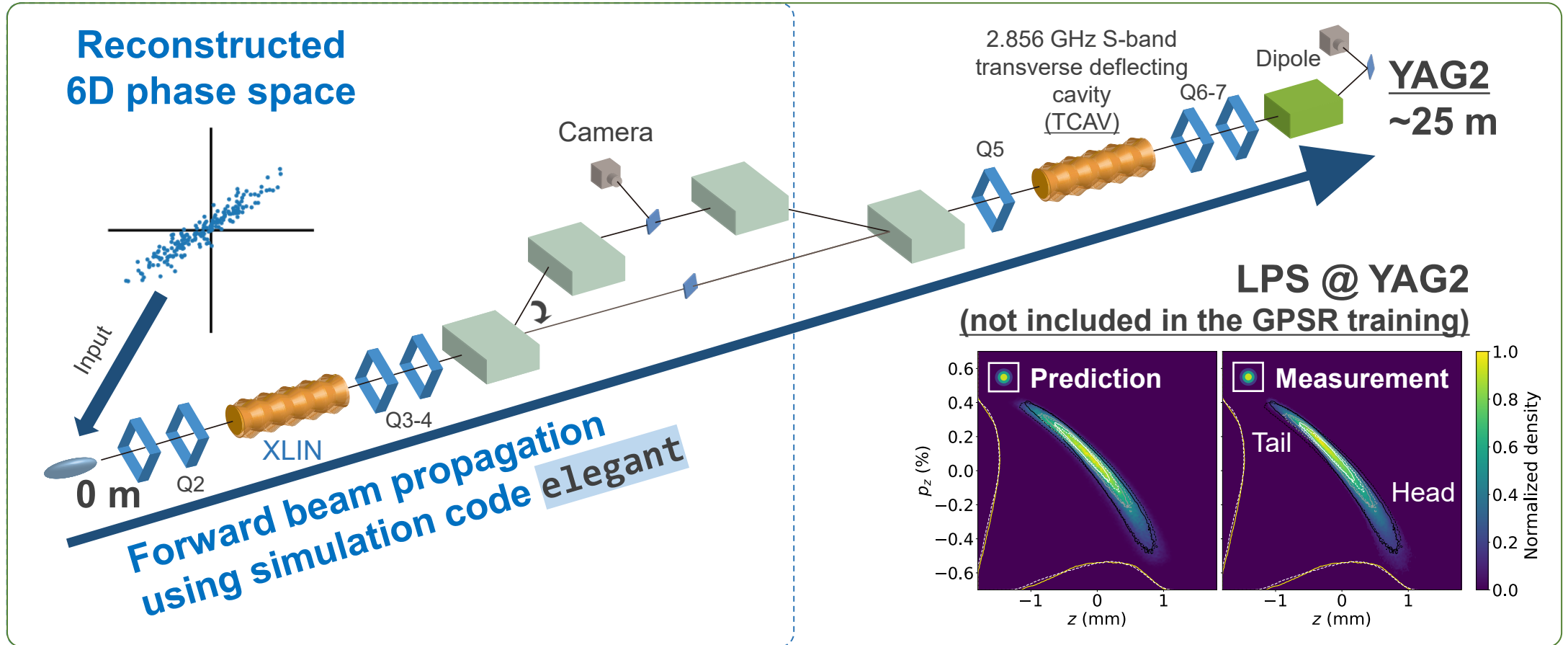
Comparison of training and test datasets @ YAG1

Training dataset

— Measurement
 Prediction



GPSR validation using downstream measurements



6D reconstructed phase space of the beam:

➔ Can be used to predict the phase space at downstream beamline

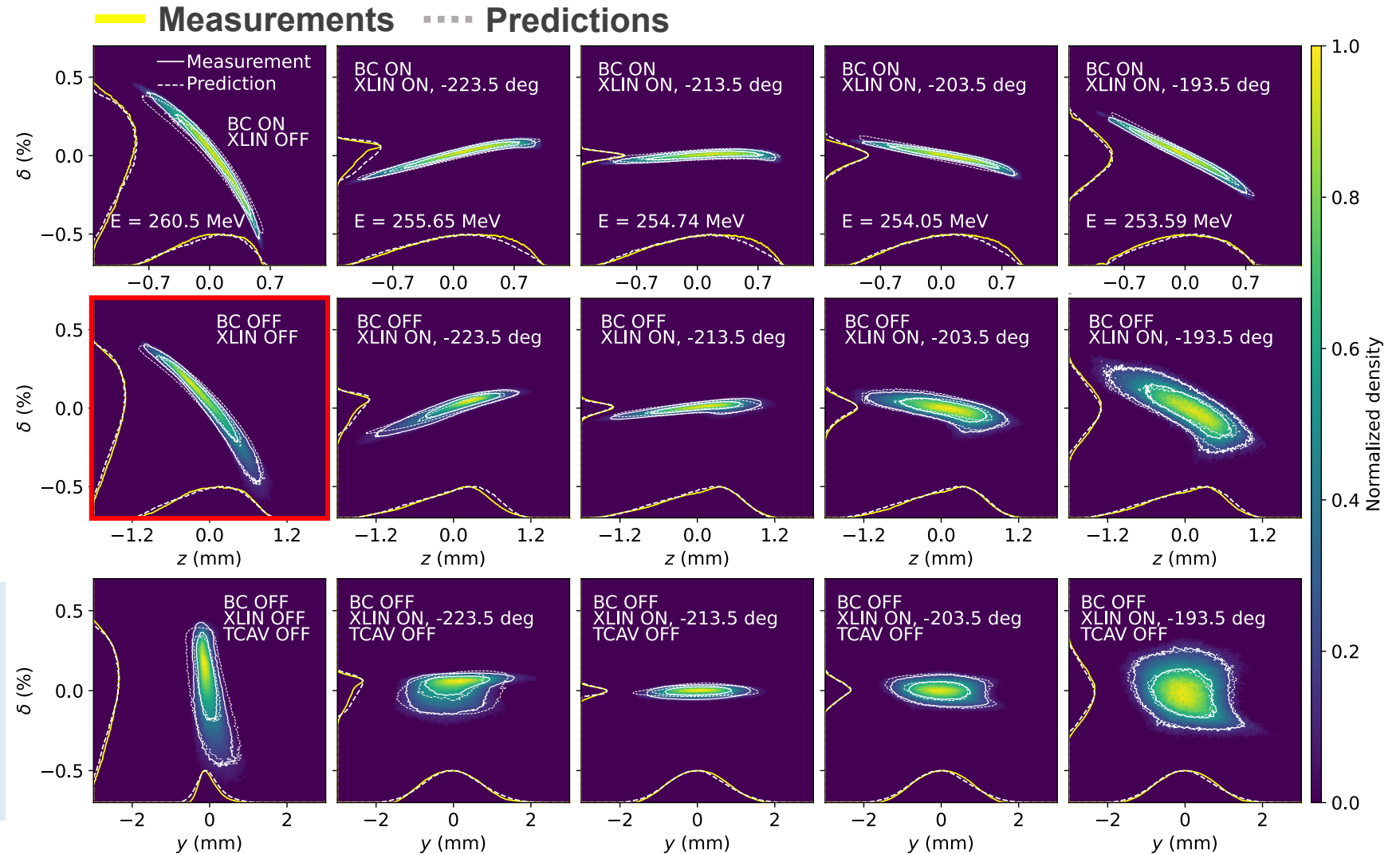
Predictions using reconstructed phase space @ YAG2



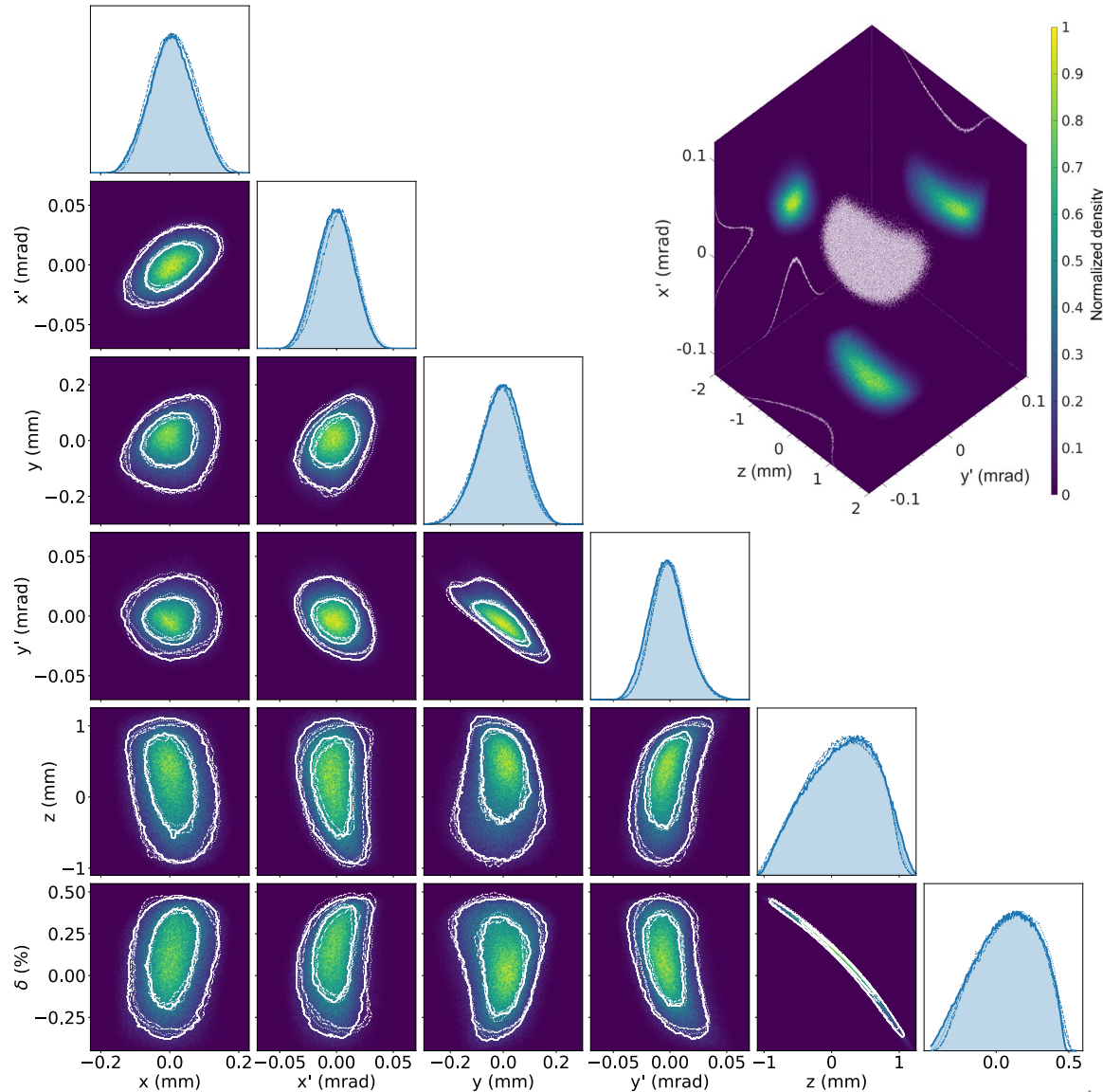
Beam image:
Measurement

Measurements
Predictions

GPSR also successfully predicts independent downstream measurements!



Reconstructed phase space @ Q1 entrance

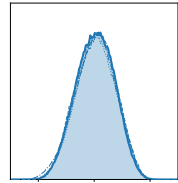


Parameters	4D Reconstruction	6D reconstruction
β_x (m)	4.59 ± 0.08	4.51 ± 0.07
β_y (m)	7.65 ± 0.11	7.81 ± 0.10
α_x (rad)	-0.55 ± 0.02	-0.52 ± 0.05
α_y (rad)	1.18 ± 0.02	1.15 ± 0.06
ϵ_{nx} (mm mrad)	0.43 ± 0.01	0.43 ± 0.01
ϵ_{ny} (mm mrad)	0.41 ± 0.01	0.41 ± 0.02

Parameters	Measurement	6D reconstruction
ϵ_{nz} (mm mrad)	137.34 ± 17.240	143.36 ± 3.87
σ_z (mm)	0.45 ± 0.01	0.46 ± 0.00
σ_δ (%)	0.24 ± 0.01	0.22 ± 0.00
Slice σ_δ (%)		0.01 (typical)

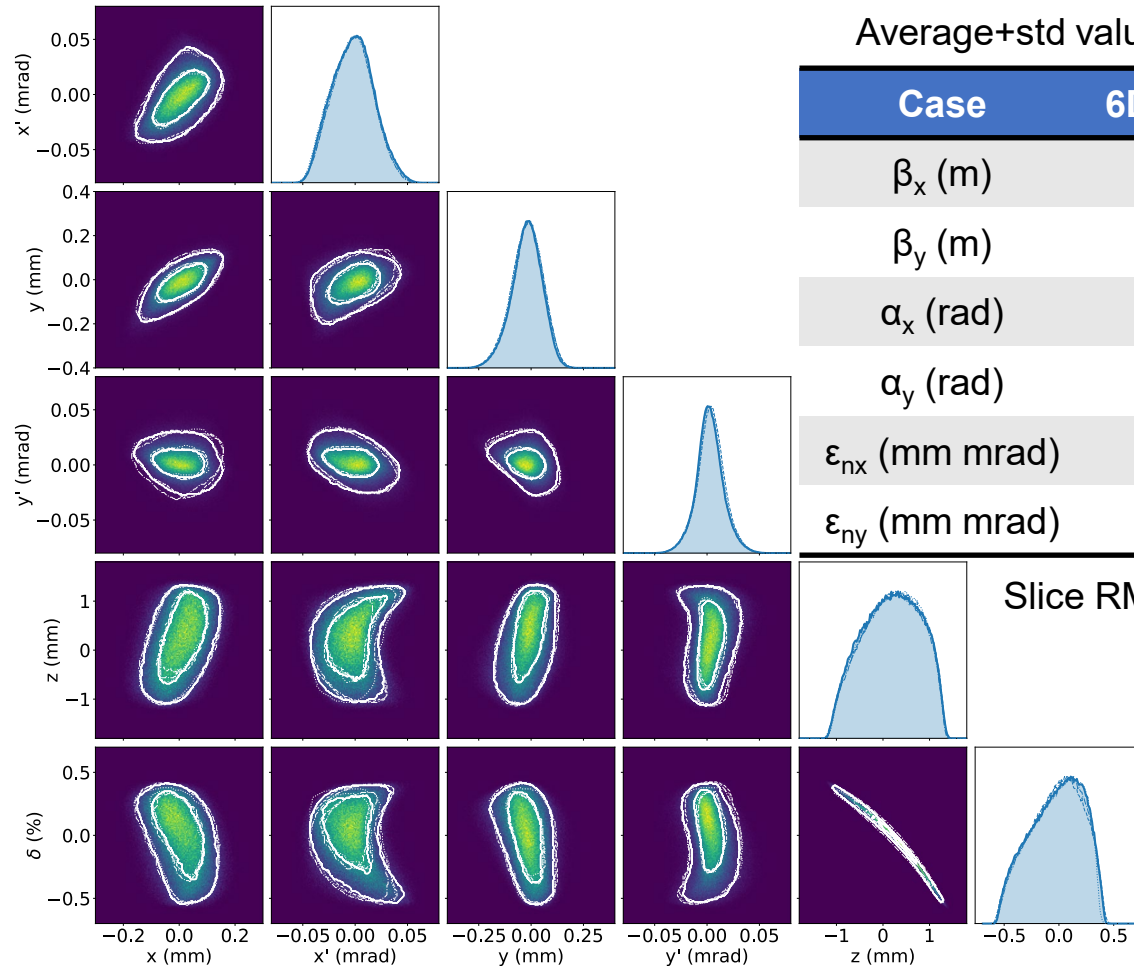
More information from 6D GPSR

➤ March 2026 measurement, preliminary analysis



Major change in operation

Gun phase: 33.7 deg ➔ 36.0 deg

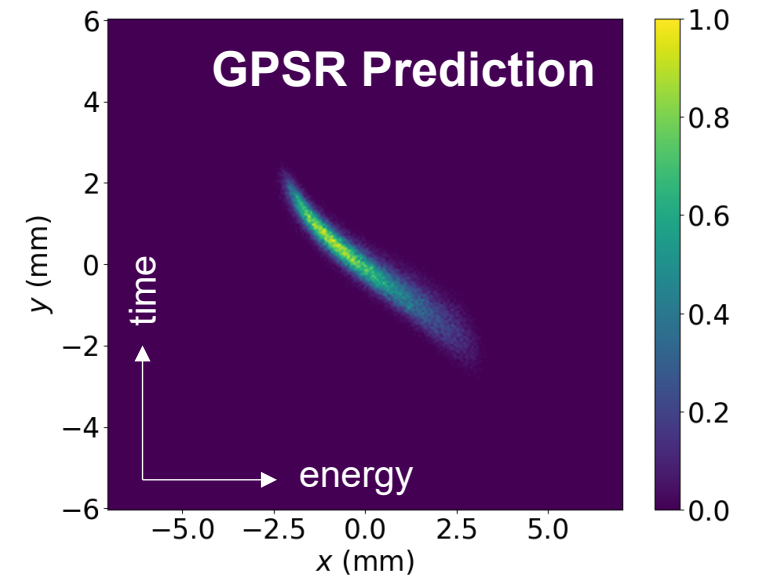
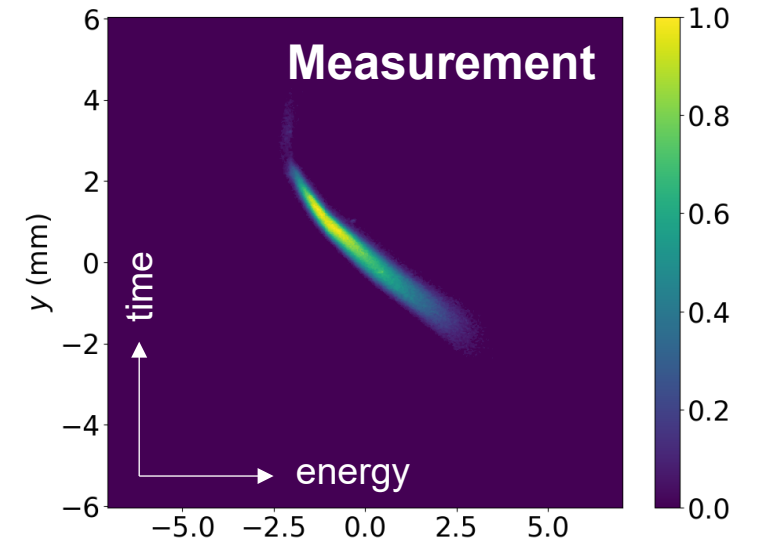


Average+std value from 15 iterations

Case	6D reconstruction
β_x (m)	4.28 ± 0.19
β_y (m)	5.96 ± 0.18
α_x (rad)	-0.60 ± 0.03
α_y (rad)	0.37 ± 0.03
ϵ_{nx} (mm mrad)	0.57 ± 0.011
ϵ_{ny} (mm mrad)	0.45 ± 0.013

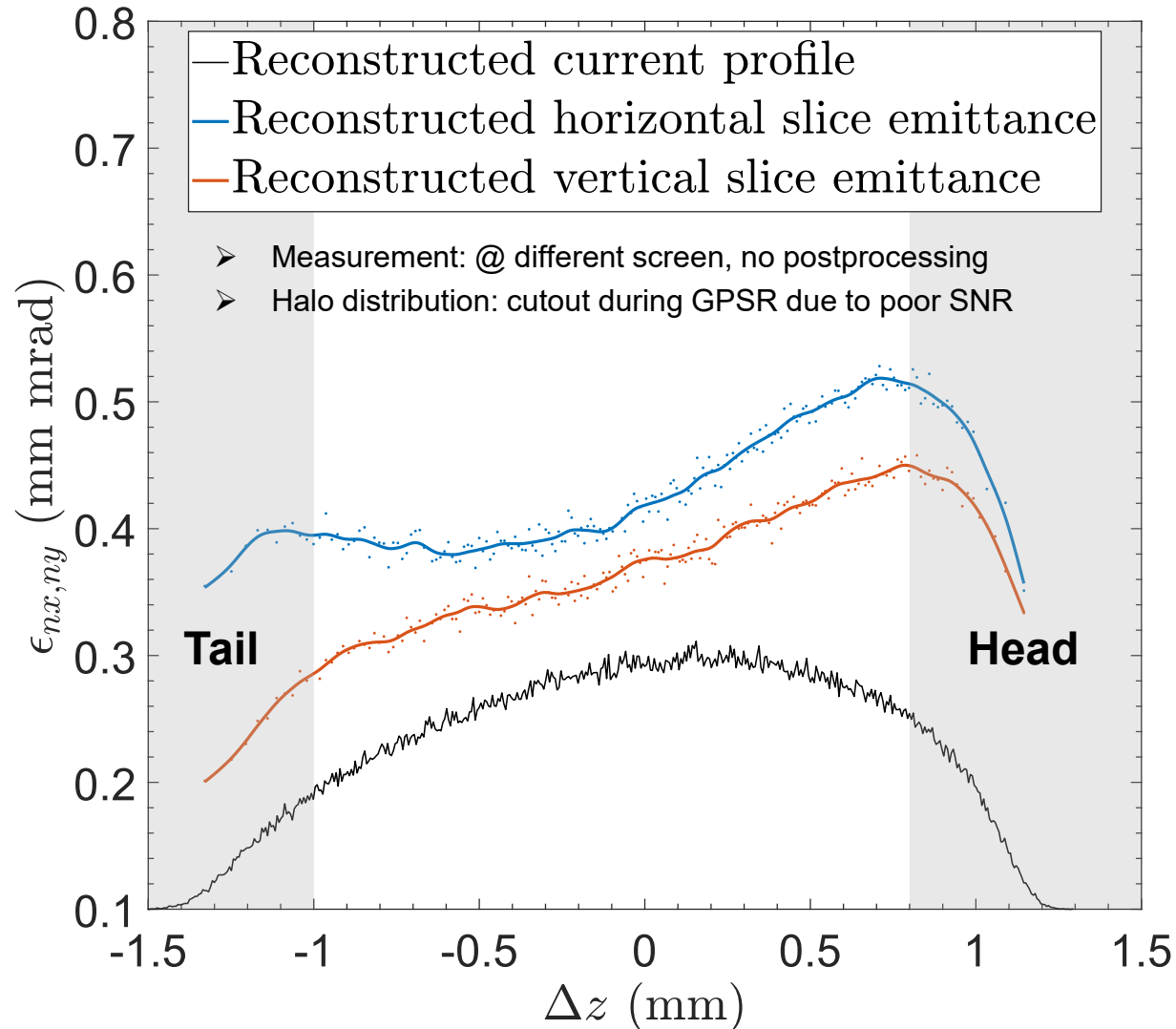
Slice RMS energy spread:
0.01%

Longitudinal phase space: (x,y) projection



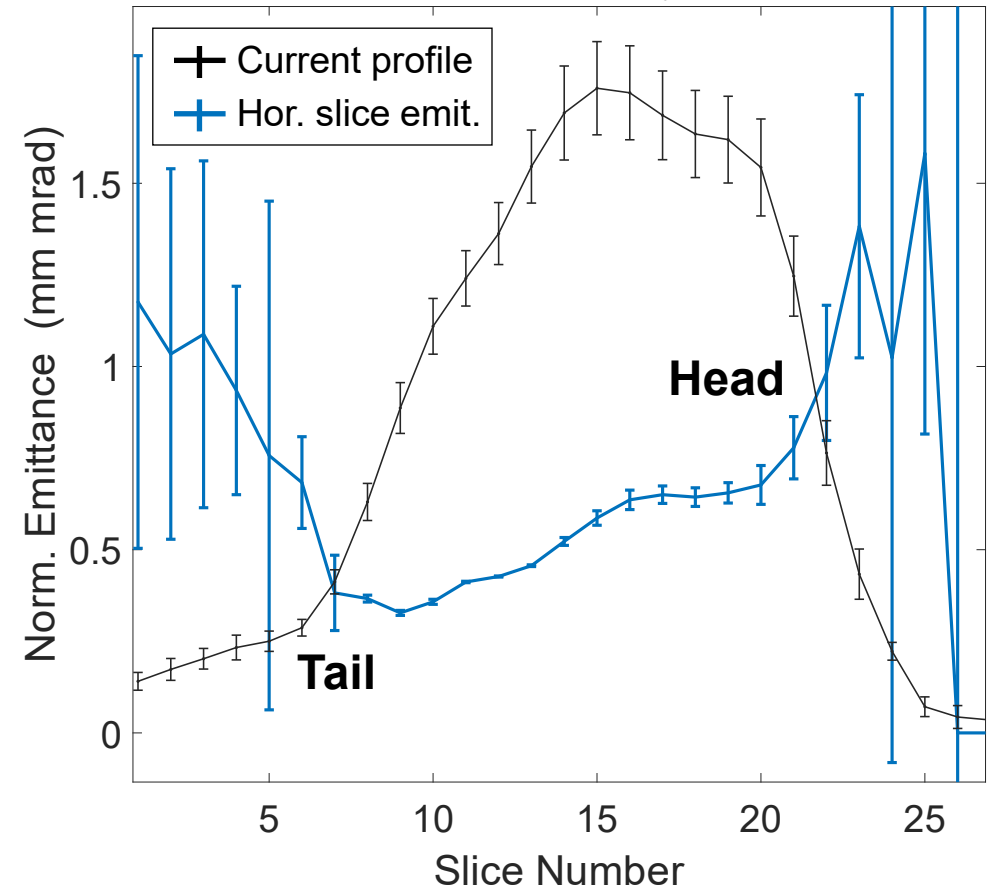
More information from 6D GPSR: x/y slice emittances

➤ March 2026 measurement, preliminary analysis



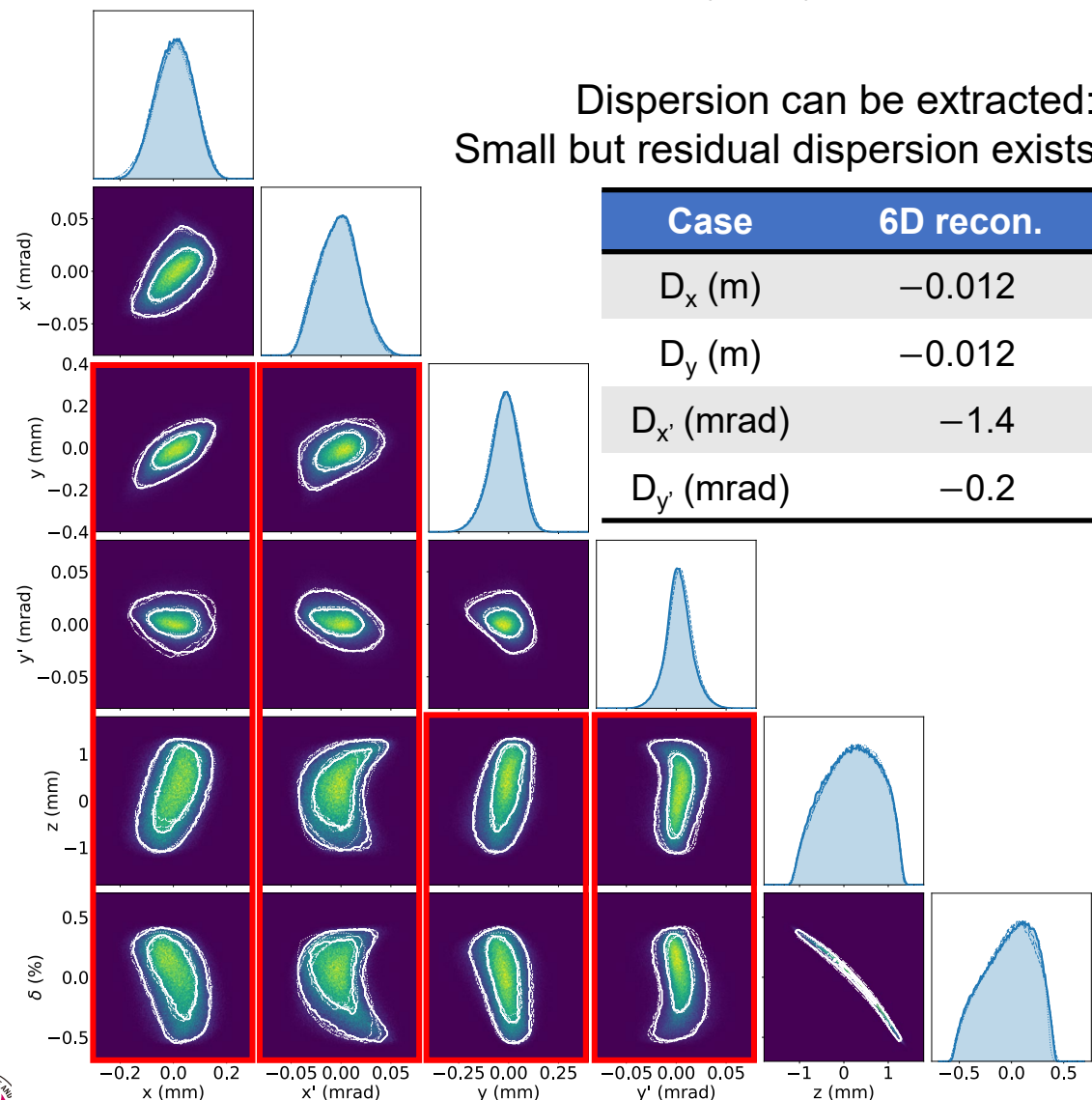
Conventional slice emittance measurement @ different screen (using TCAV)

Slice Emittance Scan on HL1:SCM11
16-Mar-2026 08:16:04 Asymmetric



More information from 6D GPSR: dispersion, correlations

➤ March 2026 measurement, preliminary analysis



For $\mathbf{X} = (x, x', y, y', z, \delta)$,

Pearson correlation coefficient:
$$\rho(i, j) = \frac{\langle X_i X_j \rangle}{\sqrt{\langle X_i^2 \rangle \langle X_j^2 \rangle}}$$

Coefficient close to ± 1 : strongly correlated*

Coefficient for reconstructed phase space

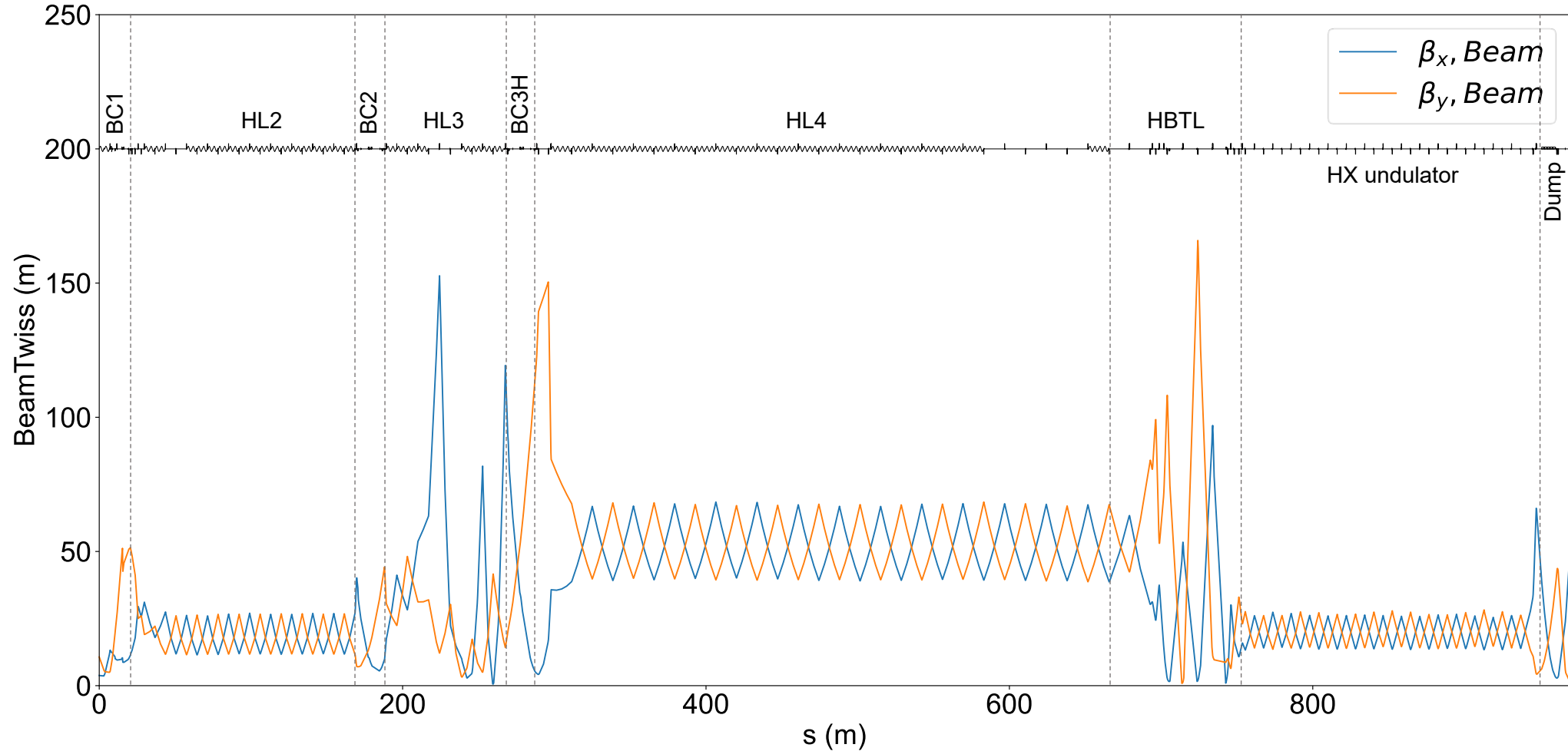
$$\rho_{\mathbf{X}} = \begin{bmatrix} 1.000 & 0.516 & 0.673 & -0.089 & 0.425 & -0.400 \\ 0.516 & 1.000 & 0.455 & -0.430 & 0.152 & -0.174 \\ 0.673 & 0.455 & 1.000 & -0.351 & 0.378 & -0.365 \\ -0.089 & -0.430 & -0.351 & 1.000 & 0.061 & -0.029 \\ 0.425 & 0.152 & 0.378 & 0.061 & 1.000 & -0.988 \\ -0.400 & -0.174 & -0.365 & -0.029 & -0.988 & 1.000 \end{bmatrix}$$

For ideal impact+elegant simulations, correlations are typically in the order of 0.001

This information from the GPSR can be used for the optimization of beam correlations

Applications using 6D GPSR: beamline optimizations

- elegant simulation used



GPSR-based beam diagnostics ➡ optimization ➡ calibrated model-based digital twin*

Summary and future works

- **Beam manipulation becomes gradually important**
 - Manipulation of cross-plane correlation, nonlinear chirp and double horn, final focus with certain shape, for high-energy physics applications and high-brightness X-ray light
- **GPSR-based phase space reconstruction was successfully demonstrated both at test and user facilities**
 - All the coupled phase spaces can be successfully predicted also for special beams
 - readily applicable using common elements such as RF cavity, quad, dipole, and screen
 - Near unique solution: can represent the physical ground truth
 - Optimization of the beamline using 6D GPSR results, incorporated into physics simulations
- **PAL-XFEL enhancement will be carried out**
 - Beam diagnostics using the GPSR technique will be performed @ PAL-XFEL to investigate the machine condition: measurement-based model calibration can be performed
 - Therefore, measurement-based optimization using calibrated model can be performed to maximize the FEL quality and on-line virtual diagnostics

Acknowledgements



Haeryong Yang
Myung-Hoon Cho
Kookjin Moon

Seongyeol Kim
Chi Hyun Shim
Hoon Heo

Gyujin Kim
Chang-Kyu Sung

Auralee Edelen
Ryan Roussel

We also thank the PAL-XFEL accelerator control team members and Prof. Moses Chung of POSTECH

Juan Pablo Gonzalez-Aguilera (now @ SLAC)
Young-Kee Kim

John Power Scott Doran Gongxiaohui Chen
Philippe Piot Wanming Liu Eric Wisniewski Charles Whiteford
(previously @ NIU)

- This work was supported by the National Research Foundation of Korea (NRF) grant (2019R111A1A01041573, RS-2024-00347026, RS-2024-00455499), funded by the Korea government (MSIT).
- This work was also supported by the U.S. Department of Energy, Office of Science under Contract No. DE-AC02-06CH11357 and No. DE-AC02-76SF00515 and the Center for Bright Beams, NSF award PHY-1549132.
- This research used resources of the National Energy Research Scientific Computing Center (NERSC), a U.S. Department of Energy Office of Science User Facility located at Lawrence Berkeley National Laboratory, operated under Contract No. DE-AC02-05CH11231 using NERSC award BES-ERCAP0020725.



Pohang Accelerator Laboratory

80 Jigokro-127-beongil,
Nam-gu, Pohang,
Gyeongbuk 37673, Republic of Korea

